FINAL REPORT ~ FHWA-OK-15-02

# FIELD PERFORMANCE MONITORING AND MODELING OF INSTRUMENTED PAVEMENT ON I-35 IN McCLAIN COUNTY

**Nur Hossain, P.E.**
**Dharamveer Singh, Ph.D.**
**Musharraf Zaman, Ph.D., P.E.**
**School of Civil Engineering and Environmental Science**

**Md. Ridwanul Alam**
**S. M. Shazzad S. Rassel**
**School of Electrical and Computer Engineering**

**College of Engineering**
**The University of Oklahoma**

**David Timm, Ph.D., P.E.**
**National Center for Asphalt Technology**
**Civil Engineering Department**
**Samuel Ginn College of Engineering**
**Auburn University**

**April 2015**

Oklahoma Department of Transportation

# FIELD PERFORMANCE MONITORING AND MODELING OF INSTRUMENTED PAVEMENT ON I-35 IN McCLAIN COUNTY

**FINAL REPORT ~ FHWA-OK-15-02**
ODOT SP&R ITEM NUMBER 2200

**Submitted to:**
John R. Bowman, P.E.
Director of Capital Programs
Oklahoma Department of Transportation

**Submitted by:**
Nur Hossain, P.E.
Dharamveer Singh, Ph.D.
Musharraf Zaman, Ph.D., P.E.
Md. Ridwanul Alam
S. M. Shazzad Rassel
*The University of Oklahoma*

David Timm, Ph.D., P.E.
*National Center for Asphalt Technology*

Oklahoma Department of Transportation

**April 2015**

**TECHNICAL REPORT DOCUMENTATION PAGE**

| 1. REPORT NO. | 2. GOVERNMENT ACCESSION NO. | 3. RECIPIENT'S CATALOG NO. |
|---|---|---|
| FHWA-OK-15-02 | | |

| 4. TITLE AND SUBTITLE | 5. REPORT DATE |
|---|---|
| Field Performance Monitoring and Modeling of Instrumented Pavement on I-35 in McClain County | Apr 2015 |
| | 6. PERFORMING ORGANIZATION CODE |

| 7. AUTHOR(S) | 8. PERFORMING ORGANIZATION REPORT |
|---|---|
| Nur Hossain, Dharamveer Singh, Musharraf Zaman, Md. Ridwanul Alam, S. M. Shazzad Rassel, and David Timm | |

| 9. PERFORMING ORGANIZATION NAME AND ADDRESS | 10. WORK UNIT NO. |
|---|---|
| College of Engineering, The University of Oklahoma 202 West Boyd St. #107, Norman, Oklahoma 73019,and<br>Department of Civil Engineering, Auburn University 238 Harbert Engineering Center, Auburn, Alabama 36849 | 11. CONTRACT OR GRANT NO.<br>ODOT SP&R Item Number 2200 |

| 12. SPONSORING AGENCY NAME AND ADDRESS | 13. TYPE OF REPORT AND PERIOD COVERED |
|---|---|
| Oklahoma Department of Transportation<br>Capital Programs Division<br>200 N.E. 21st Street, Room 3A7<br>Oklahoma City, OK 73105 | Final Report<br>Oct 2012 - Dec 2014 |
| | 14. SPONSORING AGENCY CODE |

15. SUPPLEMENTARY NOTES

16. ABSTRACT

Phase 1 of this project was conducted to better understand the cause of pavement failure under actual traffic loading and environmental conditions. A 1,000-ft. long experimental pavement section was constructed on I-35 in McClain County and was instrumented for field data collection. The test section was designed to fail in a relatively short period of time under heavy interstate traffic. After approximately four years (from 2008 to 2012) of exposure to continuous interstate traffic and environment, the test section experienced significant rutting but no fatigue cracking. Therefore, the funding agency decided to monitor the test section for two additional years (from 2012 to 2014) as part of Phase 2 of the project. Additionally, a need for predicting distresses (i.e., rut, based on the site-specific data) using the Mechanistic Empirical Pavement Design Guide (MEPDG) software was expressed. In Phase 2 of this project, the quarterly field testing (FWD, rut measurements, roughness measurements, and crack mapping) was performed on a quarterly basis. Also, the weekly downloading of traffic data and data processing were performed to allow updating of the rut prediction models developed in Phase 1 of this study. Site-specific (Level 1) input parameters for traffic, climate and materials were developed in this study. Furthermore, the rut prediction models in the MEPDG software were calibrated using the developed input parameters and measured rut depths from the test section. Laboratory tests (Hamburg rut, four point beam fatigue, volumetric properties, etc.) were performed on the extracted samples from the test section. Moreover, the contribution of different pavement layers to total rutting was assessed by a forensic investigation involving cutting full-depth trenches at three selected locations of the test section.

| 17. KEY WORDS | 18. DISTRIBUTION STATEMENT |
|---|---|
| Mechanistic-Empirical, Calibration Coefficients, Rut, Fatigue, IRI, FWD, Forensic, WIM, Hamburg | No restrictions. This publication is available from the Capital Programs Div., Oklahoma DOT. |

| 19. SECURITY CLASSIF. (OF THIS REPORT) | 20. SECURITY CLASSIF. (OF THIS PAGE) | 21. NO. OF PAGES | 22. PRICE |
|---|---|---|---|
| Unclassified | Unclassified | 64 | N/A |

# SI* (MODERN METRIC) CONVERSION FACTORS

| APPROXIMATE CONVERSIONS TO SI UNITS | | | | |
|---|---|---|---|---|
| **SYMBOL** | **WHEN YOU KNOW** | **MULTIPLY BY** | **TO FIND** | **SYMBOL** |
| **LENGTH** | | | | |
| **in** | inches | 25.4 | millimeters | mm |
| **ft** | feet | 0.305 | meters | m |
| **yd** | yards | 0.914 | meters | m |
| **mi** | miles | 1.61 | kilometers | km |
| **AREA** | | | | |
| **$in^2$** | square inches | 645.2 | square millimeters | $mm^2$ |
| **$ft^2$** | square feet | 0.093 | square meters | $m^2$ |
| **$yd^2$** | square yard | 0.836 | square meters | $m^2$ |
| **ac** | acres | 0.405 | hectares | ha |
| **$mi^2$** | square miles | 2.59 | square kilometers | $km^2$ |
| **VOLUME** | | | | |
| **fl oz** | fluid ounces | 29.57 | milliliters | mL |
| **gal** | gallons | 3.785 | liters | L |
| **$ft^3$** | cubic feet | 0.028 | cubic meters | $m^3$ |
| **$yd^3$** | cubic yards | 0.765 | cubic meters | $m^3$ |
| NOTE: volumes greater than 1000 L shall be shown in $m^3$ | | | | |
| **MASS** | | | | |
| **oz** | ounces | 28.35 | grams | g |
| **lb** | pounds | 0.454 | kilograms | kg |
| **T** | short tons (2000 lb) | 0.907 | megagrams (or "metric ton") | Mg (or "t") |
| **TEMPERATURE (exact degrees)** | | | | |
| **$^oF$** | Fahrenheit | 5 (F-32)/9<br>or (F-32)/1.8 | Celsius | $^oC$ |
| **ILLUMINATION** | | | | |
| **fc** | foot-candles | 10.76 | lux | lx |
| **fl** | foot-Lamberts | 3.426 | candela/$m^2$ | $cd/m^2$ |
| **FORCE and PRESSURE or STRESS** | | | | |
| **lbf** | poundforce | 4.45 | newtons | N |
| **$lbf/in^2$** | poundforce per square inch | 6.89 | kilopascals | kPa |

| APPROXIMATE CONVERSIONS FROM SI UNITS | | | | |
|---|---|---|---|---|
| **SYMBOL** | **WHEN YOU KNOW** | **MULTIPLY BY** | **TO FIND** | **SYMBOL** |
| **LENGTH** | | | | |
| **mm** | millimeters | 0.039 | inches | in |
| **m** | meters | 3.28 | feet | ft |
| **m** | meters | 1.09 | yards | yd |
| **km** | kilometers | 0.621 | miles | mi |
| **AREA** | | | | |
| **$mm^2$** | square millimeters | 0.0016 | square inches | $in^2$ |
| **$m^2$** | square meters | 10.764 | square feet | $ft^2$ |
| **$m^2$** | square meters | 1.195 | square yards | $yd^2$ |
| **ha** | hectares | 2.47 | acres | ac |
| **$km^2$** | square kilometers | 0.386 | square miles | $mi^2$ |
| **VOLUME** | | | | |
| **mL** | milliliters | 0.034 | fluid ounces | fl oz |
| **L** | liters | 0.264 | gallons | gal |
| **$m^3$** | cubic meters | 35.314 | cubic feet | $ft^3$ |
| **$m^3$** | cubic meters | 1.307 | cubic yards | $yd^3$ |
| **MASS** | | | | |
| **g** | grams | 0.035 | ounces | oz |
| **kg** | kilograms | 2.202 | pounds | lb |
| **Mg (or "t")** | megagrams (or "metric ton") | 1.103 | short tons (2000 lb) | T |
| TEMPERATURE (exact degrees) | | | | |
| **$^oC$** | Celsius | 1.8C+32 | Fahrenheit | $^oF$ |
| **ILLUMINATION** | | | | |
| **lx** | lux | 0.0929 | foot-candles | fc |
| **$cd/m^2$** | candela/$m^2$ | 0.2919 | foot-Lamberts | fl |
| **FORCE and PRESSURE or STRESS** | | | | |
| **N** | newtons | 0.225 | poundforce | lbf |
| **kPa** | kilopascals | 0.145 | poundforce per square inch | $lbf/in^2$ |

*SI is the symbol for the International System of Units. Appropriate rounding should be made to comply with Section 4 of ASTM E380.

## ACKNOWLEDGEMENT

The authors wish to express their sincere appreciation to John Bowman, David Streb, Jeff Dean, Bryan Hurst, Kenneth Hobson and Chris Westland, all from ODOT, for their direct and indirect assistance with this project. Bryan Cooper from ODOT deserves special thanks for his considerable contributions during the construction and instrumentation phase of this project. He also played a key role in arranging quarterly field testing. The FWD testing and data analysis assistance received from Scott Cosby and Christopher Clarke of ODOT are greatly appreciated. The authors are thankful to Rouzbeh Ghachi, Manik Barman and Debaroti Ghosh for their assistance and support during the laboratory testing phase of this project.

# Table of Contents

## List of Tables



## List of Figures

# 1.0 BACKGROUND

The Phase 1 (Item 2200) of this project was undertaken to document the field performance (rut, fatigue, roughness) of the instrumented pavement section located on the southbound lane of I-35 near Purcell, Oklahoma. A 1,000-ft test section was constructed and instrumented with earth pressure cells, asphalt strain gages, temperature probes, moisture sensors, and lateral position sensors to monitor performance under real traffic loading and environmental conditions. Real-time traffic data was collected by a weigh-in-motion (WIM) station, located about three-quarters of a mile south of the instrumented section. A weather station was installed to collect temperature, rainfall, wind and other weather data. The asphalt layers were under-designed with the anticipation that the pavement section would experience fatigue failure within few years, allowing monitoring of performance throughout the service life of the pavement. The field data collection was focused on pavement performance data (e.g., distribution of stresses within the pavement structure, longitudinal and transverse strains at the bottom of the asphalt layer, rutting, cracking), environmental data (e.g., air temperature, variation of temperature within the pavement structure), and traffic data (e.g., axle load, position, speed). In addition, field evaluations were conducted quarterly including falling weight deflectometer (FWD) testing, rut measurements at six selected transverse sections, and crack mapping. Since the rut profile measured on the pavement surface results from rutting of different layers within the pavement structure, a decision was made by the Project Panel to conduct a forensic investigation of the relative contribution of each layer through full-depth trenching toward the end of the project. A need for predicting distresses (i.e., rutting, based on the site-specific data) using the Mechanistic Empirical Pavement Design Guide (MEPDG) software was expressed by the Oklahoma Department of Transportation (ODOT). Subsequent discussions between the Capital Programs Division and Division 3 personnel revealed that the agency did not have enough funds for the reconstruction. A follow-up meeting between the ODOT personnel and the OU team was held on September 12, 2012 to discuss the preferred options for this project in moving forward. It was noted that it might take between twelve to eighteen months to find resources for the reconstruction of the

test section. Consequently, it was decided to extend this project for two additional years as Phase 2 of the original project. It is to be noted that Phase 1 of this project has already been completed, and a final report has been submitted to ODOT (Solanki, 2010).

In Phase 2 of this project, the quarterly field testing (FWD, rut measurements, roughness measurements, and crack mapping) has been performed on a quarterly basis. Also, the weekly downloading of traffic data and data processing have been performed to allow updating of the rut prediction models developed in Phase 1. To assist the agency in the implementation of the MEPDG efficiently, site-specific (Level 1) input parameters for traffic, climate and materials were developed in this study. Furthermore, the rut prediction models in the MEPDG software were calibrated using the developed input parameters and measured rut depths from the test section. Laboratory tests (i.e., Hamburg rut, fatigue, and volumetric properties) were performed on the extracted samples from the test section. Moreover, to determine the contribution of different pavement layers to total rutting, a forensic investigation was performed by cutting full-depth trenches at three selected stations of the test section. This report contains the accomplishments of Phase 2.

# 2.0 OVERVIEW OF WORK DONE

## 2.1 Task 1: Weekly Downloading and Processing of Traffic Data

Continuous traffic data collected by the WIM station were downloaded weekly and were processed for the composition, axle loads and other features, as done throughout Phase 1. Sometime after May 15, 2014, the OU project team started encountering problems in connecting and downloading traffic data from the WIM station. The OU project team worked closely with the ODOT personnel to resolve the issue. On July 16, 2014 the funding agency notified the OU project team that the data collection system at the WIM station had gone out of order. ODOT's technical personnel tried to fix the data collection equipment but were unable to make the necessary repairs. It was also notified that ODOT was not planning to replace the equipment since the project was nearing an end. Therefore, the continuous WIM data could be collected only

through May 15, 2014. However, pavement temperature data were collected monthly throughout the duration of Phase 2.

## 2.2 Task 2: Quarterly Field Testing and Processing of Data

### *2.2.1 Field Rut Measurements*

A total of eight field trips were conducted during the project period (Phase 2) to address pavement distresses. These included rutting, fatigue cracking, and surface roughness. During the field trip on October 28, 2013, a total of 20 cylindrical samples and six slab samples were extracted from the test section for laboratory testing. Trenching activities were performed in the last field trip for the project on October 7, 2014. During the field surveys, rut measurements were conducted at six selected stations, that included Station No. 144, 235, 319, 540, 738 and 900. Rut data were collected across the wheel paths at each station using a Face Dipstick® with 12-in. moon-foot spacing. The rut progression graphs for all the test sections are presented in Figure 1. Figure 1 shows six rut progression curves, each curve representing the rutting progression at a specific station. The first three points of each curve (pertaining to August 21, 2008, December 3, 2008 and January 8, 2009) present the highest rut depth measured with the straight edge/rut gauge combination method. The rest of the points on each curve (from May 19, 2009 to July 21, 2014) present the highest rut values of the two wheelpaths measured with the Face Dipstick®. On October 6, 2014, rut measurements were performed on only three stations targeted for the trenching activities: Station No. 235, 738 and 900. From Table 1, it can be seen that the rut depths data, collected during the project period (from October 2012 to October 2014), have generally increased for all stations. The increase in rutting varied between 0.010-in. to 0.156-in. The highest recorded rut value is 0.868-in. (22.05-mm), recorded on October 6, 2014 at Station No. 738. From these observations, in general, it can be concluded that the rut depths increased from October, 2012 through 2014, especially during warmer months. Field rut measurements show that all stations in the I-35 test section have undergone both primary rutting and secondary rutting. No tertiary rutting was observed at any station. Similar type of rutting behavior was observed at the AASHO road test (Finn. et al., 1977) and NCAT Test Track (Selvaraj, 2007). Finn et al. (1977)

and Selvaraj (2007) reported visible increase in rut depth values during summer and fall months, but not in winter months. Thus, the observations from the present study are in agreement with those from the AASHO road test and the NCAT studies. Further discussions of field rut test results are presented in Hossain (2010).

### *2.2.2 Field Crack Mapping*

Crack mapping was performed for the entire test section during the quarterly field trips. For Station No. 144, 319, 540, 738 and 900, crack mapping was performed over a distance of 50-ft. each way (north and south) at each station, except Station No. 235. To eliminate overlapping of mapping area, crack mapping was performed at 41-ft. north and 34-ft. south of Station No. 235. Pavement cracks were observed on the test section during the field trip in July, 2014, for the first time in approximately 6 years of service life and after approximately 4.3-million ESAL of traffic loading. Some of the cracks were longitudinal while the others were transverse. Figure 2 shows some of the cracks and their approximate locations. All the cracks were located within approximately 4 feet from the starting point of the test section to approximately 132-ft. of the test section. No visual cracks were observed elsewhere in the test section. To investigate whether the cracks on the test section are top-down or bottom-up or temperature cracks, it was decided to extract full-depth pavement core samples from the cracked locations. During the October, 2014 field trip, some cracked locations were marked on the pavement and full-depth samples were obtained using a core-rig (Figure 3). It was observed from the core samples that the cracks were only at the surface, not evident below the pavement surface (i.e., not a top-down or bottom-up crack). Therefore, one can conclude that the observed cracks may be either temperature cracks or very premature top-down cracks in nature.

### *2.2.3 FWD Testing and Analysis*

A Dynatest model 8000 series (8002-057) type Falling Weight Deflectometer (FWD) was used in this study. The FWD testing was conducted at six stations located at an interval of approximately 100-ft. along the test section. FWD tests were conducted by following ASTM D4694 test methods (ASTM, 2009). For conducting FWD tests on the top of asphalt layer, an 11.8-in. diameter plate was used with seven deflection sensors

spaced at 8, 12, 24, 36, 48, and 72-in. from the center. The loading pattern included three seating drops plus one load drop from different heights in progressive order. The FWD testing was conducted on the top of the asphalt layer for four different loads (6, 9, 12 and 15 kips). The collected data was analyzed for layer modulus values using a widely used software, MODULUS 6.0 (Liu, W. and Scullion, T., 2001). The asphalt modulus-temperature correlation is presented in Figure 4. The regression analysis of the back-calculated data from FWD testing yielded an exponential best-fit line of the form presented in Equation (1) with $\alpha_1$ = regression constant (8,849 ksi), $\alpha_2$ = regression constant (–0.035), and T = mid-depth temperature of the total asphalt layers, obtained from the temperature sensors (ºF).

$$E = \alpha_1^{\alpha_2 T} \quad (1)$$

In general, Equation (1) is a good predictor ($R^2$ = 0.82) of modulus value of asphalt at different temperatures. In Figure 4, the back-calculated modulus of asphalt-layer and pavement temperature correlations are presented. As noted above, these modulus values were obtained from the FWD tests conducted on the test section. More than six years of data (from May, 2008 through July, 2014) are presented in this figure. Figure 5 represents the back-calculated asphalt-concrete modulus and pavement temperature correlations from the beginning of the I-35 (Phase 1) project to the beginning of Phase 2. From Figure 5, it can be observed that the $\alpha_1$ value for the best-fit line is 8,785-ksi and the $\alpha_2$ value is –0.035. Therefore, one can conclude that the test section's stiffness did not change significantly over the two years of the I-35 (Phase 2) project (i.e., from May, 2012 to July, 2014).

### *2.2.4 International Roughness Index (IRI)*

The IRI for the test section was evaluated using the Face Dipstick®. These data were collected at Station No. 319, spanning 50-ft. north and 50-ft. south and at three different locations, namely inner wheel path, outer wheelpath and mid-lane. The mid-lane IRI value is obtained from the test section for comparison purposes. The IRI results are presented in graphical and tabular forms in Figure 6 and Table 2, respectively. Based on the graph in Figure 6, the average IRI value of the two wheelpaths at the

section started around 70s and increased almost continuously over time. The highest average IRI value observed on the test section was 154. In general, the IRI values increased with time, which means that the road surface was getting rougher with time, as expected. Based on the Federal Highway Administration standard (FHWA, 2013), the pavement at the test section is now considered in 'mediocre' condition (IRI value between 120 and 170).

## 2.3 Task 3: Updating Rut Prediction Models and Comparing Predicted and Measured Ruts

In this study, two different rut prediction models were developed from the traffic and environmental data obtained from the instrumented test section. One model was a Vertical Strain-based (VSB) model and the other was a Shear Strain-based (SSB) model. A commonly used multilayered linear elastic analysis software, WinJULEA, was used to predict strains induced by vehicular traffic on the test section. Approximately 30.8-million axles have passed through the test section over the six-year period (from May, 2008 to July, 2014). During this period, a total of approximately 4.7-million ESAL (Equivalent Single Axle Load) was recorded on the test section. Rut measurements, made approximately every three months, were linearly interpolated to have a rut value for each hour of each day. As rutting was measured at six selected stations, each set of values were averaged to obtain one rutting value for that field trip. By relating the measured hourly rutting to the strains induced by vehicular traffic on the test section, the rut prediction model was developed by performing a nonlinear regression analysis using the least–square method. An Excel spreadsheet was used for this purpose. Detailed discussions on the methodology and development of rut prediction models are presented by Hossain (2013).

### *2.3.1 Updated Vertical Strain-based (VSB) Model*

The updated form of the VSB rut prediction model is given in Equation (2).

$$\mathrm{Rut_i} = \mathrm{Rut_{i-1}} + 9.11 \times 10^{-07}(\mathrm{N_{si}}^{1.00\times10^{2}\varepsilon_{si}} + \mathrm{N_{ti}}^{4.15\times10^{2}\varepsilon_{ti}}) \qquad (2)$$

where:

$Rut_i$ = Rut at time 'i' from field measurements,

$Rut_{i-1}$ = Rut at time 'i-1' from field measurements,

$\varepsilon_{si}$ = Average hourly vertical strain from steering axles,

$\varepsilon_{ti}$ = Average hourly vertical strain from tandem axles,

$N_{si}$ = Total number of steering axle passes at time 'i', and

$N_{ti}$ = Total number of tandem axle passes at time 'i'.

WinJULEA analyses showed that, for a particular vehicular load, the maximum vertical strain is experienced on the top of the aggregate base layer. So, vertical strain on the top of the aggregate base layer was used to develop the vertical strain-based rut prediction model. When rut was predicted using the developed VSB model [Equation (2)], the $R^2$ value, based on the comparison between the predicted and the measured rut values, was found to be 0.78. Further, the positive coefficients for both traffic and vertical strains indicate that an increase in the number of axle passes and strain levels will increase rutting, as expected. Figure 7 shows the predicted rutting obtained from the VSB model and the measured average rutting of all stations, as a function of the cumulative number of axles.

### *2.3.2 Updated Shear Strain-based (SSB) Model*

The updated form of the SSB rut prediction model is given in Equation (3).

$$\mathrm{Rut_i} = \mathrm{Rut_{i-1}} + 8.85 \times 10^{-07}(\mathrm{N_{si}}^{8.46\times10^{2}\gamma_{si}} + \mathrm{N_{ti}}^{2.49\times10^{2}\gamma_{ti}}) \qquad (3)$$

where:

$\gamma_{si}$ = Average hourly shear strain from steering axles, and

$\gamma_{ti}$ = Average hourly shear strain from tandem axles.

The approach to compute shear strain was similar to the approach to compute vertical strain. However, the shear strain was computed at different depths in the HMA layer using WinJULEA. Depending upon the vehicle weight, the maximum shear strain was observed at the tire's edge and at a depth of about 0.5-in. (12.7-mm) to 2-in. (51-mm) below the pavement surface. When rut was predicted using the developed shear

strain-based model [Equation (3)], the $R^2$ value, based on the predicted and measured rut values, was obtained as 0.72. Based on the $R^2$ values, both regression models (VSB and SSB) are expected to predict rut at this site with a similar level of effectiveness. Further, the positive coefficients for both traffic and shear strains indicate that an increase in the number of axle passes and strain levels will increase the rutting, as expected. Figure 8 shows the predicted rutting from the shear strain-based model and the measured rutting from the test section as a function of increasing number of axles.

## 2.4 Task 4: Collecting Pavement Samples and Conducting Laboratory Testing

### *2.4.1 Extraction and Collection of Field Samples*

During the field trip on October 28, 2013, the OU project team, with the help of the ODOT personnel, extracted cylindrical and block samples from the pavement to conduct performance tests in the laboratory. A total of 20 full-death cylindrical core samples (approximately 6-in. in diameter and 7-in. in height) were obtained from the wheelpaths and mid-lane of the test section from 5 different stations. Samples were not obtained from the instrumented station (Station 319) to avoid potential damage to the instrumentation from the extraction activities. The cores were obtained using 6¼ inch O.D. diamond core barrel operated from a drill rig. Locations of the core and block samples are shown in Figure 9 and Figure 10. A total of 6 block samples were extracted from the shoulders of the test section from Station No. 540, 738 and 900. The block samples were obtained using saw-cutting machine. Figure 11 and (a)

(b)

Figure 12 show the pavement sample extraction activities.

### *2.4.2 Rut Tests on Field Samples*

Quarterly field rut measurements on the test section showed that out of the six stations, Station No. 738 consistently showed the highest rut while Station No. 900 showed lowest rut. A total of 12 samples were obtained from these two stations: 4 from wheelpaths and 8 from middle of wheelpaths. Although, a total of four cylindrical core samples were obtained from the wheelpaths of these two stations (two samples each

from a station), it was decided that only the samples obtained from the middle of the wheelpaths would be tested for laboratory rutting susceptibility. It was hypothesized that the samples from the wheelpaths have already experienced significant rutting throughout the pavement life, whereas, the samples from the middle of the wheelpaths may not have experienced any rutting or much smaller rutting. Therefore, laboratory rut tests were conducted on samples obtained from the middle of the wheelpaths in these two stations. Full depth pavement cores were extracted from these locations, however, only the top S4 layer was tested for rutting in the Hamburg Wheel Tracking machine.

#### 2.4.2.1 Hamburg Wheel Tracking (HWT) Test

As mentioned earlier, the core samples obtained from the field were approximately 7-in. in height, of which approximately 2-in. from the S4 layer (½-in. NMS Superpave mixture) and approximately 5-in. from the S3 layer (¾-in. NMS Superpave mixture). The S4 and S3 layers were visually marked on each core. Then the S4 and S3 layers were separated using the saw cutting machine available in the Broce laboratory at OU. Then the S4 samples were tested for air voids using the OHD L-14 test methods (ODOT, 2014). The HWT tests were conducted following OHD L-55 test method (ODOT, 2014). Cylindrical specimens of 6-in. diameter and 2.36-in. height is required for testing in the HWT machine. As the S4 layers were approximately 2-in. in height, Plaster of Paris was used at the bottom of the extracted S4 cores to bridge the gap between the specimen and the HWT mold. Further, two specimens were cut from the side to match the HWT plastic mold dimensions, and were used as one set. Cores from Station No. 738 are marked as 11, 12, 13 and 14, whereas the cores from Station No. 900 were marked as 17, 18, 19 and 20. For convenience, samples 11 and 12 constitute Set-1, samples 13 and 14 constitute Set-2, samples 17 and 18 constitute Set-3, and samples 19 and 20 constitute Set-4. The test procedure requires that the cylindrical samples be secured in the device, using plastic molds. During testing, the 1.85-in. wide wheel is tracked across a sample submerged in a water bath at 50±1°C temperature under 20,000 passes or until a rut depth of 20 mm. The load on the wheel is 158-lbs. (705-N). The average speed of the wheel is approximately 0.68-MPH (1.1-km/hour); and travels approximately 9.05-in. (230-mm) before reversing the direction. The device

operates at approximately 53±2 wheel passes/min. Rut depths were measured continuously with a LVDT. Figure 13 shows the HWT device used in this study.

Figure 14 shows a representative set of samples from the HWT test. Figure 15 (a through d) shows graphical views of the maximum and minimum ruts observed for the four sets after the HWT tests. This can also be observed from Figure 15 that no moisture induced damage was evident for Set-1 and Set-2 samples, while Set-3 and Set-4 samples exhibited some moisture induced damage (stripping). Detailed analyses of stripping are beyond the scope of this study.

Table 3 presents a summary of the result from the HWT tests. It can be observed from the table that the maximum and minimum rut values from these tests were 4.2-mm and 1.5-mm, respectively. Set-2 showed the minimum rut, whereas Set-4 showed the maximum rut. The variations in maximum and minimum rut depths in the samples were not very significant. For example: there is only 0.2-mm variation in minimum rut depths and 0.8-mm variation in the maximum rut depths. Overall, it can be noted that the HWT test results show no significant difference in rut depths on the extracted samples from the test section. This should also be mentioned here that the rut tests were performed on extracted pavement samples which have experienced significant environmental exposure over the past six years and therefore have gone through significant aging. This could also explain the difference in rutting depths observed in the field versus the HWT rutting depths on the samples.

### *2.4.3 Four Point Beam Fatigue Test*

The block samples were extracted from the shoulder at Station No. 540, 738 and 900, for laboratory beam fatigue tests. Two block samples were obtained from each location. The locations of block samples were marked on the pavement and cuts were made using a masonry saw. However, the extraction of block samples was tricky, as each block sample was approximately 20-in. long x 5-in. wide x 7-in. thick and weighed approximately 60 lbs. A brick tong was used to extract the blocks without any damage. The extracted blocks were further saw-cut to achieve the specific dimensions (15-in. long x 2.5-in. wide x 2-in. thick) for beam fatigue testing of the S3 layers.

A total of 10 samples were tested in the Four Point Beam Fatigue test apparatus. Each beam specimen was subjected to cyclic loading and unloading with a frequency of 10-Hz, inside a temperature chamber at 20°C, as recommended by AASHTO T321 (AASHTO, 2010). Figure 16 shows the setup for Four Point Beam Fatigue test. In this study, the beam fatigue tests were conducted at a deflection level of 400 micro-strain. A 5-kN (1100-lbf.) load cell was used to measure the loads applied to the beam specimen. An LVDT with a maximum stroke length of ±1-mm (0.04-in.), mounted on a target glued at the center of the beam was used to measure the vertical deformation of the beam. The initial stiffness was determined at the $50^{th}$ load cycle. The total number of load repetitions leading to a 50% reduction in the initial stiffness was considered as the test termination criterion, and was reported as the fatigue life (AASHTO, 2010). Figure 17 shows a representative beam specimen after fatigue testing. Table 4 presents a summary of the fatigue test results.

From Table 4, one can observe that the initial stiffness of the beam samples, obtained from three different stations, varied from approximately 8,800-MPa to 11,500-MPa. It may also be noted that the beam fatigue tests were also performed on the extracted samples from the virgin test section in 2009 (Solanki et al., 2013). Initial stiffness observed from the fatigue tests on virgin pavement samples varied from approximately 3500-MPa to 4700-MPa. Therefore, it can be noted that the stiffness of the test section have increased by approximately 2.5 times.

## 2.5 Task 5: Forensic Investigation through Trenching

To further investigate the nature and extent of rutting and to examine the contribution of different structural layers to the total rutting, trenches were cut at three selected locations on the test section. The following locations were used for this purpose: Station No. 235, 738 and 900. Station No. 738 had the highest rutting, while Station No. 900 exhibited the lowest rutting. Rutting observed on Station No. 235 was somewhat in the average range of the test section. Therefore, it was decided to cut trenches at these three stations to capture the highest, lowest and average rutting of the test section.

The trenching operations for the project were performed on October 7, 2014. The trenching operation started around 8:30 a.m. and was finished around 3:30 p.m. The OU and ODOT personnel, along with Dr. David Timm from Auburn University, were involved in the trenching operations. The following tasks were performed:

1) The trench locations were first marked on the test section (Figure 18). At first, the research team discussed the possibility of trenching the entire width of the lane. However, as the test section is located on the right lane of the two-lane Interstate-35 southbound, trenching of the entire width did not seem to be a safe approach. Therefore, the research team decided to trench approximately half of the lane starting from the shoulder, to capture the rutting contribution of the outside wheelpath on the test section. As the rut depths were very similar in the inside and outside wheel path, trenching activities to capture rutting of the outside wheelpath seemed an efficient and safer approach.
2) Approximately 10-ft.x3-ft. trenches were cut using a wet-saw cutting machine (Figure 19) at Station No. 235, 738 and 900. Depths of the trenches were approximately 36 to 42 inches. The test section is comprised of approximately 7 inches of asphalt layer (2-in. of S-4 and 5-in. of S-3 layers), 8 inches of aggregate base layer and 8 inches of stabilized subgrade layer over natural subgrade soil. The pavement layers were removed from the trenches using a Caterpiller® 22-in. wide back-hoe and a jack-hammer (Figure 20).
3) After the slabs had been removed, the trench edges and faces were cleaned using a garden hose. The Face Dipstick® with 12-in. moonfoot spacing was then used to measure the surface profile on each side of the trench (Figure 21) and an average surface profile for each trench was determined. The locations of the moonfoots were marked on the pavement.
4) Depths of each lift in the pavement layers were visually marked on each face of the trench (Figure 22). Then, depths of each pavement layer (including each lift), from the respective surface, were measured using a carpenter square and a leveler (Figure 23). The depths were measured at the marked moonfoot spacing locations. Measurements were taken at 8 locations in each trench.

5) Then the measured depths of the layers in the two faces of the trench were averaged to report one single depth at each point. It was decided to measure the rut profile by construction lift thicknesses. Therefore, for each trench there were measurements for one S4 layer, two S3 layers, and one aggregate base layer. Figure 24, Figure 25 and Figure 26 represent the rut profile of each pavement layer at stations 235, 738 and 900, respectively.

### *2.5.1 Contribution of Different Layers to Rutting*

It can be observed from Figures Figure 24 through Figure 26 that almost all of the movements are confined to only the surface layer, which is the S4 layer in the test section. Although, few movements were observed in the subsequent S3 and aggregate base layers, the movements did not align with the wheelpaths, as it was for the top S4 layer. As the movements in the S3 and aggregate base layers do not follow a consistent pattern like the S4 layer and because the movements are not significant, it can be concluded that the movements in the S3 and aggregate base layers are mere construction anomalies as can be expected in any pavement construction. Therefore, it can be concluded that no significant contributions were observed from other layers, and the rutting at the test section was primarily contributed by the 2-in. thick surface layer (S4 layer).

Forensic investigations were undertaken by different groups of researchers to investigate the contributions of different pavement layers to rutting. Two notable references in this category are NCHRP Report 468 (NCHRP, 2002) and NCAT Report 12-07 (Timm et al., 2012). The shape of the pavement profile observed after rutting in the I-35 test section was very similar to the shape of rutted pavement profile in the NCHRP study, where the HMA layer or the aggregate base layer was the primary contributor to rutting. Also, the I-35 test section includes a stabilized subgrade layer above the natural subgrade layer to minimize the contribution of subgrade layer to rutting. Based on the aforementioned observations, one could conclude that the rut in the test section was contributed primarily by the HMA layer, and more specifically by the S4 layer.

## 2.6 Task 6: Distress Modeling Using MEPDG Software

### *2.6.1 Introduction to MEPDG*

Most state DOTs are gradually shifting pavement design approach from the 1993 AASHTO design method to the Mechanistic Empirical Pavement Design Guide (MEPDG) approach. The AASHTO 1993 empirical design method is based on the limited data obtained from the AASHO road test in 1960s involving one particular environment with one particular set of materials and traffic (Muthadi and Kim, 2008). Comparatively, the MEPDG is a product of research studies involving more than 20 years of data from different regions, climatse and materials. Consequently, the MEPDG is believed to better predict pavement performance through better utilization of local materials, traffic conditions and regional climate, compared to the 1993 AASHTO design guide method (Flintsch et al. 2008; Souliman et al., 2010).

However, to gain the full benefit of pavement design using the MEPDG can be a challenging task. The MEPDG has three different input categories: (1) traffic, (2) climate and (3) materials. It also has three different levels of input data: Level 1, Level 2 and Level 3. Level 1 inputs provide the highest level of accuracy and, therefore, would have the lowest level of uncertainty or error. Level 1 inputs require site-specific data based on field and laboratory tests. Level 2 inputs provide an intermediate level of accuracy. Level 2 inputs are typically user-selected. These inputs could come from an agency database, could be derived from a limited testing program, or could be estimated using correlations. Level 3 inputs provide the lowest level of accuracy. Therefore, it is desirable to develop Level 1 inputs for the most accurate design.

The MEPDG software has various distress prediction models, such as rutting and fatigue models. Even if Level 1 inputs are developed, the pavement distress prediction models in the MEPDG needs to be calibrated to incorporate local conditions. The purpose of incorporating local calibration in MEPDG is to addressany differences in construction practices, traffic and environmental conditions, maintenance policies, and material specifications across the United States (Metha et al., 2008). Although the MEPDG design method predicts pavement performance from laboratory-developed performance models, the models need to be adjusted based on the observed

performance in the field to reflect the differences between predicted and actual field performance. The MEPDG rut models have been calibrated globally using the data obtained from the Long Term Pavement Performance (LTPP) test sections throughout North America (Aguiar-Moya et al., 2008). Therefore, to implement these models efficiently, it is necessary to calibrate the MEPDG rut models for local materials, traffic and environmental conditions.

### *2.6.2 MEPDG Rut Models*

Permanent deformation or rutting is one of the major distresses in flexible pavements. One of the objectives of this study was to calibrate the MEPDG rutting models from the data obtained from the I-35 test section. The MEPDG uses the incremental damage concept to predict total rut depth in a pavement structure. The total rut depth is calculated as the summation of rut depths accumulated in all unbound (loose) and bound (asphalt and/or cement/asphalt-treated base) layers. Equation 4 is used in the MEPDG to calculate total rut depth (RD):

$$RD = \sum_{i=1}^{n} \varepsilon_{p,i} h_i \quad (4)$$

where:

n = Total number of sublayers,

i = Sublayer number,

$\varepsilon_{p,i}$= Plastic strain in sublayer i, and

$h_i$ = Thickness of sublayer i.

Equations 5 and 6 show the permanent deformation (rut) models in the MEPDG for asphalt layers and for unbound base and subgrade layers, respectively:

$$\frac{\varepsilon_p}{\varepsilon_r} = K_z \beta_{r1} 10^{k_{r1}} T^{\beta_{r2} k_{r2}} N^{\beta_{r3} k_{r3}} \quad (5)$$

where:

$\varepsilon_p$ = Plastic strain (in./in.),

$\varepsilon_r$ = Resilient strain (in./in.),

$T$ = Temperature of layer at middepth (°F),

$N$ = Number of load repetitions,

$\beta_{r1}, \beta_{r2}, \beta_{r3}$ = Local calibration coefficients,

$k_{r1}, k_{r2}, k_{r3}$ = National coefficients ($k_{r1}$ = -3.35412, $k_{r2}$ = 1.5606, $k_{r3}$ = 0.4791), and

$K_z$ = Depth confinement factor that adjusts the permanent strain for the confining pressure.

$$\delta_a = \beta_{s1} k_1 \varepsilon_v h \left(\frac{\varepsilon_0}{\varepsilon_r}\right) \left| e^{-\left[\frac{\rho}{N}\right]^{\beta}} \right| \quad (6)$$

where:

$\delta_a$ = Permanent deformation for the layer,

$\varepsilon_v$ = Average vertical strain (in./in.),

$h$ = Thickness of the layer,

$\varepsilon_0$,$\beta$, ρ = Material properties, and

$\beta_{s1}$ = Calibration coefficient to optimize for both base and subgrade layers.

Therefore, the total rut of a pavement section is the summation of the rut occurring in each layer [the Granular Base coefficient ($k_{GB}$) = 2.03 and the Subgrade coefficient ($k_{SG}$) = 1.35}:

$$RD = h_{AC} \varepsilon_r K_z \beta_{r1} 10^{k_{r1}} T^{\beta_{r2} k_{r2}} N^{\beta_{r3} k_{r3}} + \beta_{GB} k_{GB} \varepsilon_v h_{GB} \left(\frac{\varepsilon_0}{\varepsilon_r}\right) \left| e^{-\left[\frac{\rho}{N}\right]^{\beta}} \right| + \beta_{SG} k_{SG} \varepsilon_v h_{SG} \left(\frac{\varepsilon_0}{\varepsilon_r}\right) \left| e^{-\left[\frac{\rho}{N}\right]^{\beta}} \right| \quad (7)$$

where:

$h_{AC}$ = Thickness of asphalt layer,

$h_{GB}$ = Thickness of granular base layer, and

$h_{SG}$ = Thickness of subgrade layer.

It is evident that there are five calibration coefficients: $\beta_{r1}, \beta_{r2}$ and $\beta_{r3}$ for the asphalt layer, $\beta_{GB}$ for the granular base layer, and $\beta_{SG}$ for the subgrade layer.

### *2.6.3 Need for calibration of MEPDG Rut Models*

The purpose of incorporating local calibration in MEPDG is to address the differences in construction practices, traffic and environmental conditions, maintenance policies, and material specifications across the United States (Metha et al., 2008). Although, ODOT can use the performance models with nationally calibrated “default”

coefficients, the outcome may not reflect the actual field measurements. Therefore, higher level of precision and economically optimum outcomes can be achieved if transportation agencies like ODOT calibrate these rut model coefficients to represent the local conditions (traffic, materials and environment) prevalent in Oklahoma. In the present study, the MEPDG rut calibration models were calibrated using the I-35 test section's data. The calibrated model can be assumed to represent the local conditions of Oklahoma.

### *2.6.4 Overview of MEPDG Input Parameters*

#### 2.6.4.1 Traffic

The MEPDG software asks for the following traffic inputs: base year traffic volume, traffic growth rate, monthly adjustment factors, vehicle class distribution factors, hourly distribution factors, and axle load spectra, among other factors. Some of the major traffic inputs are reviewed below for completeness:

*Monthly Adjustment Factor*

The monthly adjustment factor (MAF) represents the proportion of annual truck traffic for a given class of a vehicle that occurs in a specific month. In other words, the monthly distribution factors for a specific month is equal to the monthly truck traffic for a given class for the month divided by the total truck traffic for that truck class for the entire year. The MEPDG assumes a constant MAF for the entire design period for all types of vehicles. Usually vehicles classes of 4 through 13 are used to develop MAF.

$$MAF_i = \frac{AMDTT_i}{\sum_{i=1}^{12} AMDTT_i} \times 12 \quad (8)$$

where:

$MAF_i =$ Monthly adjustment factor for month i, and

$AMDTT_i =$ Average monthly daily truck traffic factor for month i.

*Hourly Distribution Factor*

The hourly distribution factor (HDF) represents the percentage of average annual daily truck traffic (AADTT) within each hour of the day. There can be Level 1, Level 2 or

Level 3 inputs for the hourly distribution factors. The following steps are involved in generating HDF:

Step 1: Determine the total number of trucks counted within each hour of traffic data in the sample.

Step 2: Average the number of trucks for each of the 24 hours of the day in the sample.

Step 3: Total the 24 hourly averages from Step 2.

Step 4: Divide each of the 24 hourly averages from Step 2 by the total from Step 3 and multiply by 100.

*Vehicle Class Distribution*

Vehicle class distribution (VCD) is calculated from the data gathered from vehicle classification counting programs such as Automatic Vehicle Count (AVC), Weigh-In-Motion (WIM) and vehicle counts. Normalized VCD represents the percentage of each truck class (Class 4 through Class 13) through the AADTT for the base year. Default VCD is provided in the MEPDG software. The design guide lists 17 Truck Traffic Classification (TTC) groups based on the roadway function class and the traffic stream expected on a given roadway. The designer can choose the default set of TTC that suits his/her design purpose, or can use the Level 1 VCD developed from the actual traffic data for the project. The latter option gives the designer the most accurate vehicle class distribution for a particular application.

*Number of Axle/Truck*

This input represents the average number of axles for each truck class (Class 4 to Class 13) for each axle type (single, tandem, tridem and quad). The designer can use the values determined through direct analysis of site-specific data (Level 1), or regional/statewide traffic data (Level 2), or the default values based on analyses of national databases (Level 3).

*Axle Load Spectra*

The axle load distribution factors represent the percentage of total axle applications within each load interval for a specific axle type and vehicle class. Definition of load intervals for different axle types is provided below:

- Single Axles: 3 kips to 40 kips, at 1 kip interval.
- Tandem Axles: 6 kips to 80 kips, at 2 kips interval.
- Tridem and Quad Axles: 12 kips to 102 kips at 3 kips interval.

The normalized axle load spectra can only be determined from WIM data. Therefore, the level of inputs depends on data source (site, regional or national). For the design procedure, load spectra are normalized on an annual basis.

#### 2.6.4.2 Climate

One of the major advances in pavement design using the MEPDG approach over the 1993 AASHTO approach is that in the MEPDG the designer can call for specific climatic data for the particular pavement. There are numerous weather stations installed in various places throughout the US. The user can use the actual climatic data from these installed weather stations or based on the GPS coordinates of a particular location the user can call up to six nearby weather stations data and thereby generate virtual weather stations according to his/her requirements. The user can also input the climatic data from the actual data obtained from the installed weather stations.

#### 2.6.4.3 Material

This study is focused on data obtained from an instrumented flexible pavement section. Therefore, the inputs required for materials related to only flexible pavement construction are discussed here. There are three different inputs at Level 1 for asphalt concrete layer: inputs for asphalt mix, asphalt binder and asphalt in general. Dynamic modulus (E*) data for a range of temperatures and frequencies for asphalt mixes, complex shear modulus (G*) and phase angle (δ) data of the asphalt binder over a range of temperatures, and volumetric properties, such as, effective binder content, air voids and total unit weight are required as inputs at Level 1. Level 1 input for other

layers (aggregate base, stabilized subgrade, natural subgrade, etc.) utilizes the stress-dependent finite element method which has not yet been calibrated with distress. Therefore, Level 1 inputs for these layers are not yet recommended for design in the MEPDG (AASHTO, 2004). Therefore, resilient moduli data for the other layers are recommended to use at Level 3 inputs for materials in the MEPDG.

### *2.6.5 Development of MEPDG Input Parameters*

#### 2.6.5.1 Traffic

The WIM site was instrumented with inductive loops and piezoelectric sensors to capture axle configuration, weight, distance between axles, and other pertinent data for each vehicle passing through the test section. Approximately four years (from 2008 to 2012) of continuous traffic data were used to develop the traffic input parameters and axle load spectra at Level 1 for this study.

Development of traffic data inputs is a very intense analytical data reduction procedure. A commercial software, TOPS, developed by Peek Traffic Corporation, was used to reduce the continuous traffic data collected by the WIM station and then converted/saved to Microsoft Excel format (.xlsx). Because of the massive volume of these data, they were loaded from Microsoft Excel to a MySQL database for faster data processing. The column field of the MySQL database mostly comprises of date, time, vehicle class, number of axles along with their consecutive distances (i.e., distance between two consecutive axles) and their individual weights, etc. A program was written in SQL (Structured Query Language) to extract and process the data from this stored database.

From the axle definition mentioned in the FHWA vehicle classification, total number of single, tandem, tridem and quad axles were counted from the WIM data and then axles per volume was determined by dividing the total axle count by total volume. The SQL program also provides (month wise) axle weights for each axle group and for each FHWA vehicle classification. These output data were then transferred to Microsoft Excel and histograms were generated for different axle groups, on a monthly basis. The

bin ranges and intervals used to develop the histograms were recommended by the MEPDG (AASHTO, 2004).

From the WIM data, the compound traffic growth rate was found to be 2.78%. Tables Table 5 and Table 6 show the MAF and HDF that were used as Level 1 inputs in the MEPDG software. Figure 27 shows the Vehicle Class Distribution Factors that were developed from the four years of traffic data from the instrumented test section. From this figure, it is observed that the highest percentage of vehicle at this site is of Class 9 (approximately 60%) followed by Class 5 vehicles (approximately 15%). This observation is consistent with previous studies (see e.g., Tran and Hall, 2007).

Axle load spectra for four axle types (single, tandem, tridem and quad) for all vehicles were developed using the WIM data for approximately four years. As it was observed that Class 9 vehicles are predominant, among all vehicle classes, axle load distribution for Class 9 was further analyzed. Figure 28 (a) and Figure 28 (b) shows the axle load spectra for four years (2009, 2010, 2011 and 2012) for the single and tandem axles of Class 9 vehicles. It is observed from the figure that for single axles the distribution peaks around 11-kips axle loads, which is the expected range for Class 9 single axles (Tran and Hall, 2007). Extensive analyses of axle load spectra of single axles for other vehicle classes showed similar results. Table 7 shows the single axle load spectra for all the vehicle classes that traversed the test section on Interstate-35 in Oklahoma. Figure 28 (b) shows the axle load spectra for Class 9 tandem axles. It can be observed from the figure that there are two distinct peaks for the tandem axle distribution: one between 10 and 16-kips, and the other between 28 and 36-kips. Table 8 shows the tandem axle load spectra for all the vehicle classes. Some vehicle classes, e.g., Class 5 and 11 did not have tandem axles, so axle load spectra for these vehicle classes were unavailable and therefore was shown as 0.00 in Table 8.

Lateral traffic wander data was also obtained from the instrumented test section. It was found that the mean wheel location was 15.5 inches from the lane marking and the traffic wander standard deviation was 10.2 inches.

#### 2.6.5.2 Climate

The Latitude and Longitude of the instrument pavement test section are N35.045343° and W97.378348°, respectively. From these GPS coordinates, climate data were generated for the test section using the MEPDG software by interpolation of six nearby climate stations. Data from six nearby weather stations: 2 from Oklahoma City area, one weather station each from Guthrie, Lawton, Stillwater and Hobart area, were used to generate a virtual weather station for this purpose. Depth of the water table was assumed as 10-ft. (3.3-m), as was obtained from the subsurface investigation operations during the construction of the test section.

#### 2.6.5.3 Material

As discussed earlier, three different inputs are required for asphalt concrete layers: inputs for asphalt mix, asphalt binder and asphalt in general. Dynamic modulus tests were performed on the loose asphalt mixes (both S4 and S3) obtained during the construction of the test section. To determine the target air voids, field core samples were extracted from the pavement and their air voids were determined in the laboratory. Six cores were cut from each top and bottom layers of the pavement. The average air voids and standard deviation for the top layer (S4 mix) and the bottom layer (S3 mix) were 9.1% and 0.63%; and 8% and 0.42%, respectively. Therefore the target air voids for laboratory samples was considered as 9±0.5% and 8±0.5% for the top and the bottom layers, respectively. Dynamic modulus tests for both the mixes (S4 and S3) were conducted in the laboratory in accordance with the AASHTO TP62 test methods (AASHTO, 2006). Tests were performed using a mechanical testing system (MTS) equipped with a servo-hydraulic testing system (MTS, 2011). The test was conducted on each specimen at four different temperatures: -12, 4, 21, 40, and 55°C (10, 40, 70, 104 and 131°F) starting from the lowest temperature and going to the highest temperature. Though AASHTO TP62 recommends the testing of dynamic modulus on five different temperatures ranging from -10°C to 54°C, and six different frequencies: 25, 10, 5, 1, 0.5, 0.1 Hz, testing of a mix at a lower temperature is time consuming and needs a costly environmental chamber to maintain the temperature. Moreover, it causes problems in terms of ice formation inside the environmental chamber, which hinders the

testing procedure. An approach developed by Bonaquist et al. (2005) eliminates the lower temperature requirement, so that the time required in conducting dynamic modulus testing and master curve construction can be reduced. This approach uses three temperatures between 4 and 46.6°C and four frequencies between 0.01 and 10 Hz, instead of five temperatures between (-10 and 54°C) and six loading rates between 0.1 and 25 Hz, as recommended by AASHTO TP62. This Bonaquist et al. (2005) procedure was used in the present study to construct the master curve. Thus, the dynamic modulus tests were conducted at four different temperatures: 4, 21, 40, and 55°C, starting from the lowest temperature and going to the highest temperature. For each temperature level, the test was conducted at different loading frequencies from the highest to the lowest: 25, 10, 5, 1, 0.5, and 0.1 Hz. The dynamic modulus for the temperature (-10°C to 54°C) and frequencies: 25, 10, 5, 1, 0.5, 0.1 Hz recommended in AASHTO TP62 can be estimated from developed master curve. The load magnitude was adjusted based on the material stiffness, temperature, and frequency to keep the strain response within 50-150 micro-strains (Tran and Hall, 2006). The data were recorded for the last 5 cycles of each sequence. Dynamic modulus values were calculated for combinations of temperatures and frequencies. The coefficient of variation (COV) for the measured dynamic modulus values of the samples was found to be less than 15%, which satisfied the limits given in the AASHTO TP62 test method (AASHTO, 2009). The master curves were then constructed using the principle of time-temperature superposition and approach developed by Bonaquist et al. (2005). The amount of shifting at each temperature required to form the master curve describes the temperature dependency of the material. First, a standard reference temperature is selected (i.e., 21°C), and then data at various temperatures are shifted with respect to time until the curves merge into a single smooth function. Table 9 shows the dynamic modulus values for the S3 and S4 mixes at different temperature and frequencies. These values were used as inputs in the MEPDG software in this study.

Dynamic Shear Rheometer (DSR) tests were performed following ASTM D7175 tset methods (ASTM, 2008) on the PG 64-22 binder to obtain the Complex shear modulus (G*) and the phase angle (δ). DSR tests were performed in three different

temperatures: 61, 64 and 67°C (142, 147 and 152°F) for a loading rate of 1.59 Hz (10 rad/sec). Table 10 presents the binder test data used as inputs in the MEPDG software.

The other volumetric properties of the asphalt layers were obtained from the mix design sheet. Resilient Modulus ($M_r$) tests were performed on the samples from aggregate base, stabilized subgrade and natural subgrade layers (Solanki et al., 2013) in accordance with the AASHTO T 307-99 test method. The $M_r$ test consisted of applying a cyclic haversine-shaped load with a duration of 0.1 seconds and rest period of 0.9 seconds. For each sequence, the applied load and the vertical displacement for the last five cycles were measured and used to determine the $M_r$ values. The $M_r$ values obtained for the aggregate base layer were in the range of 14,234 psi to 48,569 psi. For samples from the CFA-stabilized subgrade layer, the average $M_r$ values were found to be 35,054 and 16,263-psi, at Optimum Moisture Content (OMC) and OMC+2%, respectively. The natural subgrade soil samples compacted at OMC and OMC+2% provided pavement design $M_r$ values of approximately 17,008 and 12,327-psi, respectively. The $M_r$ values used in this study as inputs in the MEPDG software are 30,000 psi and 17,008-psi for aggregate base and natural subgrade layers, respectively. As the MEPDG software is not yet calibrated for the stabilized subgrade layer, the default values were used as the inputs for the stabilized subgrade layer.

### *2.6.6 Comparison of Level 1 and Level 3 Traffic Input Parameters*

#### 2.6.6.1 Hourly Distribution Factor (HDF)

Figure 29(a) shows a graphical comparison of HDF at MEPDG Level 3 (default) and Level 1 values obtained using the CY 2009 data from the test section. The graph shows significant differences between the default and actual values obtained from the WIM station. For example, the HDFs in the default values is constant from 0 to 5 hours, then increases sharply to a value of 5 for hours 6 to 9 and increases sharply again to a value of 6. Whereas, the actual HDFs obtained from the WIM station shows a gradual increase and decrease in the HDFs. This comparison indicates that there is a need to estimate HDF for different WIM sites in Oklahoma. The variation in HDF may have significant effect on performance of a pavement during design and analysis stage.

#### 2.6.6.2 Vehicle Class Distribution (VCD)

Figure 29(b) shows a graphical comparison of VCD values between the default (Level 3) and site-specific values (Level 1) obtained from the test section for the same year. The default VCD in MEPDG is Truck Traffic Classification (TTC) group 1. When these default values were compared to the site-specific values (Level 1) obtained from the WIM station near the test section, it was observed that significant differences exist between the default and site-specific values. For example, approximately 25% difference was observed between the default and actual values for Class 9 vehicles. A difference between percentage of Class 9 and other vehicles may have significant effects on pavement performance. Therefore, it is important to have an accurate VCD factor during the pavement design and analysis phase.

#### 2.6.6.3 Monthly Adjustment Factor (MAF)

Figure 29(c) shows a graphical comparison between MEPDG default values (Level 3) for MAF and Level 1 MAF values obtained using the 2009 data from the WIM station at the test section. The default MAF value (Level 3) is constant at 1 irrespective of a month in a year, whereas the actual site-specific MAF (Level 1) values for Class 9 vehicles varied from 0.64 to 1.15 for the test section, indicating the importance of developing site-specific MAF.

#### 2.6.6.4 Axle Load Spectra

Figure 30(a) and (b) show a graphical comparison of axle load spectra between default (Level 3) and specific values (Level 1) obtained from the I-35 test section from 2009 to 2012. Only single and tandem axles for Class 9 vehicles are presented here. It is observed that the peak values of site-specific axle load distribution are higher than the default values. For example, in case of single axles, the site-specific peak value was found to be approximately 26 to 30% compared to the default value of approximately 18%. In case of tandem axles, the site-specific peak values were approximately 9% and 10% compared to the default values of approximately 8% and 6%. These graphs demonstrate the need to develop Level 1 axle load spectra for pavement design purposes.

#### 2.6.6.5 Lateral Traffic Wander

Significant difference exists between Level 1 and Level 3 lateral traffic wander data. It was found that the actual (Level 1) mean wheel location was 15.5 inches from the lane marking and the traffic wander standard deviation was 10.2 inches, compared to the default (Level 3) mean wheel location of 18 inches and the default standard deviation of 10 inches.

### *2.6.7 Calibration of MEPDG Rut Model*

Calibration was done by comparing the observed pavement performance with the MEPDG-predicted pavement performance over time. The analyses were initiated with the default (Level 3) global calibration parameters and then adjusted such that the difference between the observed and the predicted performance values was reduced progressively. The best fit minimized the difference between the observed and the MEPDG predictions.

In this study, $\beta_{r2}$ was kept constant at the value of 1, as were observed in similar studies conducted by Banerjee et al. (2009) and Hall et al. (2011). After reviewing the calibration performed by Muthdai and Kim (2008), Banerjee et al. (2009), Hall et al. (2011) and Tarefder and Rodriguez-Ruiz (2012), it was decided that a range of $\beta_{r1}$ and $\beta_{r3}$ would be chosen for the calibration effort in this study. The calibration coefficient $\beta_{r1}$ is a shift factor that modifies the intercept term of the permanent deformation model. This factor primarily captures differences in the distress predictions caused by the varying thicknesses of the HMA layers and other initial conditions. $\beta_{r3}$ captures the differences coming from the number of load repetitions. Thus, it represents the rate of permanent deformation progression.

From the literature review for the calibration coefficients of granular base ($\beta_{GB}$) and natural subgrade ($\beta_{SG}$), it was decided that the value for $\beta_{GB}$ and $\beta_{SG}$ will be assumed as 1 and 0.5, respectively, for this study. The calibration coefficients $\beta_{GB}$ and $\beta_{SG}$ capture the deviation in predictions from the observed distresses that may arise from differences in the material properties.

Trial runs were performed with multiple combinations of calibration coefficients. It was found that the rut predictions were highly sensitive to the variation of $\beta_{r3}$ and less

sensitive to $\beta_{r1}$. This is reasonable based on the fact that $\beta_{r3}$ is the calibration coefficient for the number of wheel passes and this happens to be a much bigger number than $K_z 10^{k_{r1}}$ (responsible for the initial prediction of the permanent deformation), which is accounted through $\beta_{r1}$. The model output and best fit were estimated as Sum of Squared Errors (SSE), which represents the squared sum of the differences between the observed and the predicted rut values.

Table 11 represents a total of 10 trials runs with respective SSE and $R^2$ values. It can be observed from Table 11 that combination in trial No. 10 produced the least SSE and second best $R^2$ value. Therefore, the final calibration coefficients that produced the least SSE were taken as: $\beta_{r1}$ = 2, $\beta_{r2}$ = 1, $\beta_{r3}$ = 0.9, $\beta_{GB}$ = 1 and $\beta_{SG}$ = 0.5. It should be noted that the default values of these factor at Level 3 are set as 1 in the MEPDG. The values of calibration factors obtained in this study were found to be significantly different than Level 3 (default) values. Figure 31 illustrates a visual comparison between rut predicted using the calibrated models and the measured rut from the test section. It can be seen from this figure that the difference between the MEPDG-predicted rut and actual measured rut from the field is very minimal, as the points are closer to the equality line. Student's t-test was also performed and the p-value was found to be 0.71, which is greater than 0. It means there is no significant difference between the measured and the predicted rut. The average error between the measured and the predicted rut after the calibration was less than 5%, which shows the goodness of prediction.

## 3.0 Conclusions and Recommendations

Following conclusions can be drawn from this study:

1) Field rut measurements show that all stations in the I-35 test section have undergone both primary rutting and secondary rutting. No tertiary rutting was observed in any station. After roughly six years of service, the maximum rut of 0.87-in. and the minimum rut of 0.48-in. were observed at Station 738 and Station 900, respectively. Although the rut depths increased with time, most of the rutting was accumulated during the summer months. Also, the rate of rutting

during the first summer month was much higher than in subsequent summer months with similar traffic applications.

2) A few cracks were observed from approximately 4 feet from the starting point of the test section to approximately 132-ft. of the test section. No cracks were observed elsewhere in the test section. It was observed from the extracted core samples of the cracked locations that that the cracks were only at the surface, not evident below the pavement surface (i.e., not a top-down or bottom-up crack). Therefore, the observed cracks were temperature cracks in nature. Therefore, one can conclude that the observed cracks may be either temperature cracks or very premature top-down cracks in nature.
3) The back-calculated asphalt-concrete moduli values obtained from the FWD tests did not show significant change of stiffness of the test section over the two years of the I-35 (Phase 2) project (i.e., from May, 2012 to July, 2014).
4) Field IRI values were measured using Face Dipstick®. In general, the IRI values increased with time, which means that the road surface is getting rougher with time, as expected. The highest average IRI value observed on the test section was 154. According to the FHWA guidelines, the pavement at the test section is now considered in 'Mediocre' condition.
5) Both VSB and SSB models predicted rut with similar level of accuracy, as evident from the high $R^2$ values (0.78 for VSB and 0.72 for SSB model).
6) Extracted samples obtained from the middle of the wheelpaths were tested in the HWT machine for rutting susceptibility. The maximum and minimum rut values from the tests were 4.2-mm and 1.5-mm, respectively. This can be stated that the HWT test results show there is no significant difference in rut depths on the extracted samples from the test section. This should also be mentioned here that the rut tests were performed on extracted pavement samples which have experienced significant environmental exposure over the past six years and therefore have gone through significant aging. This could also explain the difference in rutting depths observed in the field versus the HWT rutting depths on the samples.

7) Laboratory beam fatigue tests performed on the extracted samples showed that the initial stiffness of the beam samples varied from approximately 8,800-MPa to 11,500-MPa. Initial stiffness observed from the fatigue tests on virgin pavement samples (performed in the Phase 1) varied from approximately 3500-MPa to 4700-MPa. Therefore, this can be stated that the I-35 test section's stiffness have increased by approximately 2.5 times.

8) To investigate the contribution of different structural layers to pavement total rutting, full-depth trenching activities were performed in three different locations on the test section. From the trenches, it was observed that almost all of the movements are confined to only the surface S4 layer. Although the trenching activities showed some movements in the underlying pavement layers (S3 and aggregate base), those movements does not follow a consistent pattern like S4 layer and the movements were not very significant. Therefore, the S4 surface layer was found to be the only contributing layer to pavement rutting.

9) In this study, Level 1 inputs for traffic and materials were developed for the calibration of MEPDG rutting models. Significant difference was observed between Level 1 and Level 3 (default) traffic inputs. Major differences were found in the hourly distribution, monthly adjustment, and vehicle class distribution factors, as well as the axle load spectra.

10) The calibration of MEPDG rutting models is essential for prediction of an accurate field performance of a pavement. Statistical analyses performed on the calibrated models revealed no significant difference (p-value>0) between the measured and predicted rut, indicating a need of local calibration of deformation models in Oklahoma.

11) The calibration factors estimated in this paper at Level 1 were compared with the default calibration factors at Level 3. A good correlation was observed between the measured and estimated rut at Level 1, indicating the calibration significantly improves the rut prediction using the MEPDG rut models.

12) The final calibration coefficients were found to be: $\beta_{r1}$ = 2, $\beta_{r2}$ = 1, $\beta_{r3}$ = 0.9 for asphalt layers; $\beta_{GB}$ = 1 for aggregate base layer, and $\beta_{SG}$ = 0.5 for natural subgrade, while the default values of these factor at Level 3 are set to 1.

13) The sensitivity of the different calibration factors was studied and it was found that the most sensitive calibration coefficient was $\beta_{r3}$ followed by $\beta_{r1}$ related to asphalt layer.

Based on this study, the following recommendations are made for future studies:

1) Although this specific test section falls approximately in the middle of the state of Oklahoma and therefore can be considered somewhat representative for Oklahoma, a more robust calibration should be performed using the LTPP database and pavement sections available throughout Oklahoma.
2) Developed axle load spectra and other traffic input parameters should be used instead of default values for future design applications. To gain more confidence, statewide traffic input parameters should be developed using the data from all the WIM stations in Oklahoma.
3) The OU project team understands that the funding agency is planning to rehabilitate the instrumented test section in very near future. Very few research studies have been conducted on the performance of the rehabilitated pavements. As this test section was closely monitored from the beginning of the construction and/or instrumentation to the beginning of the rehabilitation phase, the funding agency should utilize a unique opportunity to monitor the performance of a rehabilitated pavement and compare that with the virgin pavement. Local calibration coefficients in the MEPDG for the rehabilitated pavement can also be developed which will be extremely helpful to ODOT in the implementation of rehabilitated pavement program.

## References


1. AASHTO (2010). “Standard Method of Test for Determining The Fatigue Life of Compacted Asphalt Mixtures Subjected to Repeated Flexural Bending”, American Association of State Highway & Transportation Officials, Washington, D.C.
2. AASHTO (2009). “Standard Method of Test for Determining Dynamic Modulus of Hot Mix Asphalt (HMA),” American Association of State Highway & Transportation Officials, Washington, D.C.
3. AASHTO (2008). Mechanistic-Empirical Pavement Design Guide – A Manual of Practice, American Association of State Highway and Transportation Officials (AASHTO), Washington, D.C.

4. Aguiar-Moya, J. P., Hong, F., and Prozzi, J. A. (2008). “Upgrading the Texas LTPP Database to Support the M-E Pavement Design Guide.” Transportation Research Board 88th Annual Meeting, CD-ROM, National Research Council, Washington, D.C.
5. ASTM (2009). “Standard Test Method for Deflections with a Falling-Weight-Type Impulse Load Device,” ASTM D4694, ASTM International, West Conshohocken, Pennsylvania.
6. ASTM (2008). “Standard Test Method for Determining the Rheological Properties of Asphalt Binder Using a Dynamic Shear Rheometer,” ASTM D7175, ASTM International, West Conshohocken, Pennsylvania.
7. Banerjee, A., Aguiar-Moya, J. P., and Prozzi, J. A. (2009). “Calibration of Mechanistic-Empirical Pavement Design Guide Permanent Deformation Models (Texas Experience with Long-Term Pavement Performance).” Transportation Research Record: Journal of the TRB, No. 2094, TRB of the National Academies, Washington, D.C. pp. 12–20.
8. Bonaquist, R., and Christensen, D.W. (2005). “Practical Procedure for Developing Dynamic Modulus Master Curves for Pavement Structural Design,” Transportation Research Record, No. 1929, Journal of the Transportation Research Board, Washington, D.C., pp. 208-217.
9. Finn, F., Saraf, C., Kulkarni, R., Nair, K., Smith, W., and Abdullah, A. (1977). “The Use of Distress Prediction Subsystems for the Design of Pavement Structures,” Proceedings of the Fourth International Conference on the Structural Design of Asphalt Pavements, Ann Arbor, Michigan, pp. 3-37.
10. Flintsch, G. W., Loulizi, A., Diefenderfer, S. D., and Diefenderfer, B. K. (2008). “Asphalt Materials Characterization in Support of Mechanistic-Empirical Pavement Design Guide Implementation Efforts in Virginia.” Transportation Research Board 87th Annual Meeting, CD-ROM, National Research Council, Washington, D.C.
11. Hall, K., Xiao, D., and Wang, K. (2011). “Calibration of the MEPDG for Flexible Pavement Design in Arkansas.” Transportation Research Record: Journal of the TRB, No. 2226, TRB of the National Academies, Washington, D.C. pp. 135–141.
12. Hoegh, K., Khazanovich, L., and Jensen, M. (2010). “Local Calibration of Mechanistic-Empirical Pavement Design Guide Rutting Model (Minnesota Road Research Project Test Sections).” Transportation Research Record: Journal of the TRB, No. 2180, TRB of the National Academies, Washington, D.C. pp. 130–141.
13. Hossain, N. (2010). “Observed and Predicted Rut Behavior of an Instrumented Test Section on I-35,” M.S. Thesis, The University of Oklahoma, Norman, OK.
14. Hossain, N., Solanki, P., Zaman, M., Muraleetharan, K. K., and Singh, D. (2013). “Development of Field Rut Prediction Models from an Instrumented Test Section on Interstate-35,” Transportation Research Board 2013 Annual Meeting, Washington D.C.
15. Li, J., Pierce, L., and Uhlmeyer, J. (2009). “Calibration of Flexible Pavement in Mechanistic-Empirical Pavement Design Guide for Washington State.” Transportation Research Record: Journal of the TRB, No. 2095, TRB of the National Academies, Washington, D.C. pp. 73–83.
16. Liu, W., and Scullion, T. (2001). “MODULUS 6.0 For Windows: User’s Manual,” Texas Transportation Institute, College Station, Texas.
17. Mehta, Y., Sauber, R., Owad, J., and Krause, J. (2008). “Lessons Learned during Implementation of Mechanistic-Empirical Pavement Design Guide.” Transportation Research Board 87th Annual Meeting, CD-ROM, National Research Council, Washington, D.C.
18. Muthadi, N., and Kim, Y. (2008). “Local Calibration of Mechanistic-Empirical Pavement Design Guide for Flexible Pavement Design.” Transportation Research Record: Journal of the TRB, No. 2087, TRB of the National Academies, Washington, D.C. pp. 131–141.

19. NCHRP Report 468 (2002), “Contributions of Pavement Structural Layers to Rutting of Hot Mix Asphalt Pavements,” Transportation Research Board- National Research Council, Washington, D.C.
20. ODOT (2014). “Method of test for Hamburg Rut testing of Compacted Hot-Mix Asphalt (HMA) – OHD L-55,” Oklahoma Highway Department, Oklahoma City, Oklahoma.
21. ODOT (2014). “Method of Test for bulk specific gravity, percent absorption, percent air voids, percent density, and longitudinal joint density in compacted dense and open graded asphalt mixtures – OHD L-14,” Oklahoma Highway Department, Oklahoma City, Oklahoma.
22. Selvaraj, S.I. (2007). “Development of Flexible Pavement Rut Prediction Models from the NCAT Test Track Structural Study Sections Data,” Ph.D. Dissertation, Auburn University, Auburn, Alabama.
23. Solanki, P., Hossain, N., Breidy, M., Singh, D., Zaman, M., and Muraleetharan, K. K. (2013). “Field Performance Monitoring and Modeling of Instrumented Pavement on I-35 in McClain County,” Final Report, The University of Oklahoma, Norman, Oklahoma.
24. Souliman, M., Mamlouk, M., El-Basyouy, M., and Zapata, C. (2010). “Calibration of the AASHTO MEPDG for Flexible Pavement for Arizona Conditions.” Compendium of Papers of the 89th TRB Annual Meeting, CD-ROM, Washington, D.C.
25. Tarefder, R., Rodriguez-Ruiz, J.I. “Local Calibration of MEPDG for Flexible Pavements in New Mexico.” Journal of Transportation Engineering, ASCE, Volume 139, Issue 10.
26. Timm, D., Robbins, M., Willis, J., Tran, N., and Taylor, A. (2012). “Evaluation of Mixture Performance and Structural Capacity of Pavements Utilizing Shell Thiopave®: Phase II: Construction, Laboratory Evaluation and Full-Scale Testing of Thiopave® Test Sections,” Final Report, National Center for Asphalt Technology, Auburn, Alabama.
27. Tran, N., and Hall, K. (2007). “Development and Influence of Statewide Axle Load Spectra on Flexible Pavement Performance,” Transportation Research Record: Journal of the Transportation Research Board, No. 2037, Washington, D.C.
28. Tran, N., and Hall, K. (2006). “An Examination of strain levels used in the dynamic modulus testing,” Journal of Association of Asphalt Paving Technologist, Vol. 75, pp. 321-343.

**Table 1: Rut Progression on the Test Section**

| Date | Highest Rut (in.) | | | | | |
|---|---|---|---|---|---|---|
| | Sta. 144 | Sta. 235 | Sta. 319 | Sta. 540 | Sta. 738 | Sta. 900 |
| 31-May-08 | 0 | 0 | 0 | 0 | 0 | 0 |
| 21-Aug-08 | 0.2 | 0.3 | **0.4** | 0.3 | 0.300 | 0.200 |
| 3-Dec-08 | 0.3 | 0.3 | **0.35** | 0.2 | 0.200 | 0.200 |
| 8-Jan-09 | 0.3 | **0.35** | 0.25 | 0.2 | 0.200 | 0.200 |
| 19-May-09 | 0.390 | **0.444** | 0.425 | 0.363 | 0.395 | 0.280 |
| 28-Oct-09 | 0.418 | 0.468 | 0.444 | 0.393 | **0.483** | 0.310 |
| 16-Feb-10 | 0.419 | 0.465 | 0.431 | 0.381 | **0.476** | 0.307 |
| 10-Mar-10 | 0.409 | 0.465 | 0.429 | 0.384 | **0.483** | 0.304 |
| 18-May-10 | 0.427 | 0.469 | 0.437 | 0.388 | **0.501** | 0.303 |
| 10-Aug-10 | 0.409 | 0.424 | 0.509 | 0.409 | **0.612** | 0.317 |
| 22-Nov-10 | 0.441 | 0.439 | 0.545 | 0.457 | **0.678** | 0.359 |
| 14-Feb-11 | 0.440 | 0.400 | 0.532 | 0.435 | **0.653** | 0.361 |
| 7-Jun-11 | 0.421 | 0.405 | 0.538 | 0.441 | **0.663** | 0.377 |
| 18-Oct-11 | 0.441 | 0.485 | 0.606 | 0.48 | **0.714** | 0.435 |
| 22-Feb-12 | 0.476 | 0.461 | 0.598 | 0.47 | **0.712** | 0.421 |
| 2-May-12 | 0.479 | 0.491 | 0.600 | 0.456 | **0.712** | 0.410 |
| 8-Nov-12 | 0.487 | 0.471 | 0.580 | 0.457 | **0.767** | 0.446 |
| 11-Apr-13 | 0.487 | 0.500 | 0.639 | 0.463 | **0.776** | 0.442 |
| 22-Jul-13 | 0.501 | 0.499 | 0.597 | 0.473 | **0.791** | 0.452 |
| 28-Oct-13 | 0.520 | 0.512 | 0.657 | 0.486 | **0.803** | 0.469 |
| 26-Mar-14 | 0.515 | 0.510 | 0.648 | 0.486 | **0.827** | 0.472 |
| 21-Jul-14 | 0.544 | 0.495 | 0.660 | 0.525 | **0.822** | 0.480 |
| 6-Oct-14 | | 0.548 | | | **0.868** | 0.476 |

Most recent recorded highest rut at the test section = 0.868 in. or 22.05 millimeter

Maximum recorded rut at the test section = 0.868 inch or 22.05 millimeter

* bold number denotes highest value recorded at that particular date of data collection

**Table 2: Average IRI Values on the Test Section**

| Date | Outer Wheel Path | Mid-Lane | Inner Wheel Path |
|---|---|---|---|
| May 19, 2009 | 65.58 | 75.72 | 75.96 |
| October 28, 2009 | 64.00 | 65.51 | 82.76 |
| February 16, 2010 | 69.26 | 73.84 | 88.98 |
| May 18, 2010 | 66.53 | 68.92 | 87.64 |
| August 10, 2010 | 69.74 | 90.94 | 77.16 |
| November 22, 2010 | 77.94 | 92.98 | 87.45 |
| February 14, 2011 | 78.05 | 130.85 | 97.57 |
| June 7, 2011 | 76.92 | 95.63 | 82.36 |
| October 18, 2011 | 77.79 | 84.09 | 93.31 |
| February 22, 2012 | 99.60 | 90.48 | 118.04 |
| May 2, 2012 | 105.45 | 100.00 | 84.53 |
| August 21, 2012 | 104.66 | 91.62 | 126.225 |
| November 8, 2012 | 138.31 | 97.68 | 110.425 |
| April 11, 2013 | 137.395 | 91.26 | 137.07 |
| July 22, 2013 | 103.81 | 86.19 | 125.46 |
| March 26, 2014 | 136.21 | 97.56 | 172.615 |
| July 21, 2014 | 179.955 | 85.64 | 109.215 |

**Table 3: Summary of the Hamburg Wheel Tracking Tests on Extracted Samples**

| Set No. | Min. Deformation (mm) | | | | Max. Deformation (mm) | | | |
|---|---|---|---|---|---|---|---|---|
| | 5,000 Cycles | 10,000 Cycles | 15,000 Cycles | 20,000 Cycles | 5,000 Cycles | 10,000 Cycles | 15,000 Cycles | 20,000 Cycles |
| 1 | 1.7 | 1.8 | 2.0 | 2.2 | 3.0 | 3.1 | 3.6 | 3.9 |
| 2 | 1.5 | 1.9 | 2.1 | 2.4 | 2.1 | 2.6 | 3.1 | 3.4 |
| 3 | 1.5 | 1.7 | 2.1 | 2.5 | 1.8 | 2.3 | 3.0 | 3.8 |
| 4 | 1.5 | 1.8 | 2.0 | 2.4 | 1.9 | 2.3 | 3.0 | 4.2 |

## Table 4: Summary of the Fatigue Test Results

| Sample ID# | Strain Level (μ $\varepsilon$) | T (°C ) | f (Hz) | Initial Stiffness (MPa) | AASHTO - Failure Cycles @50% Initial Stiffness |
|---|---|---|---|---|---|
| 540-1-1 | 400 | 20 | 10 | 10202 | 130,119 |
| 540-1-2 | 400 | 20 | 10 | 9831 | 127,751 |
| 540-2-1 | 400 | 20 | 10 | 9705 | 96,087 |
| 540-2-2 | 400 | 20 | 10 | 9732 | 150,976 |
| 738-1-1 | 400 | 20 | 10 | 11457 | 95,573 |
| 738-1-2 | 400 | 20 | 10 | 11062 | 85,746 |
| 738-2-1 | 400 | 20 | 10 | 9786 | 104,916 |
| 900-1-1 | 400 | 20 | 10 | 9751 | 104720 |
| 900-1-2 | 400 | 20 | 10 | 9183 | 79,997 |
| 900-2-1 | 400 | 20 | 10 | 8827 | 66,904 |

## Table 5: Monthly Adjustment Factors

| Month | Vehicle Class | | | | | | | | | |
|---|---|---|---|---|---|---|---|---|---|---|
| | 4 | 5 | 6 | 7 | 8 | 9 | 10 | 11 | 12 | 13 |
| January | 0.91 | 0.86 | 1.24 | 0.72 | 0.89 | 1.05 | 0.99 | 1.09 | 0.95 | 1.25 |
| February | 0.89 | 0.81 | 1.25 | 0.83 | 0.86 | 1.03 | 1.09 | 1.07 | 0.95 | 1.11 |
| March | 0.96 | 0.88 | 1.16 | 0.98 | 1.03 | 1.07 | 1.10 | 1.04 | 0.95 | 1.03 |
| April | 0.96 | 0.92 | 1.29 | 1.04 | 1.07 | 1.06 | 1.07 | 1.09 | 1.06 | 1.28 |
| May | 0.96 | 0.92 | 1.04 | 1.15 | 1.08 | 1.06 | 1.01 | 1.07 | 1.10 | 1.20 |
| June | 0.98 | 0.95 | 0.93 | 1.18 | 1.20 | 1.13 | 1.17 | 1.15 | 1.06 | 1.06 |
| July | 2.19 | 2.47 | 0.78 | 0.95 | 1.02 | 0.64 | 0.80 | 0.63 | 0.68 | 0.71 |
| August | 0.87 | 0.96 | 0.80 | 1.27 | 1.10 | 1.15 | 1.12 | 1.05 | 1.15 | 0.91 |
| September | 0.87 | 0.88 | 0.82 | 0.88 | 1.06 | 1.09 | 1.05 | 1.06 | 1.14 | 0.95 |
| October | 1.05 | 0.93 | 1.24 | 1.16 | 1.19 | 1.12 | 1.16 | 1.25 | 1.20 | 1.16 |
| November | 0.63 | 0.65 | 0.66 | 0.92 | 0.73 | 0.70 | 0.61 | 0.62 | 0.69 | 0.52 |
| December | 0.73 | 0.79 | 0.81 | 0.93 | 0.77 | 0.89 | 0.83 | 0.89 | 1.07 | 0.81 |

## Table 6: Hourly Distribution Factors

| Hour | Hourly Distribution Factor | Hour | Hourly Distribution Factor | Hour | Hourly Distribution Factor |
|---|---|---|---|---|---|
| 0 | 1.93 | 8 | 5.65 | 16 | 4.92 |
| 1 | 1.94 | 9 | 5.96 | 17 | 4.76 |
| 2 | 2.27 | 10 | 5.96 | 18 | 4.34 |
| 3 | 2.83 | 11 | 5.87 | 19 | 3.91 |
| 4 | 3.13 | 12 | 5.83 | 20 | 3.63 |
| 5 | 3.49 | 13 | 5.74 | 21 | 3.10 |
| 6 | 4.15 | 14 | 5.60 | 22 | 2.57 |
| 7 | 4.96 | 15 | 5.33 | 23 | 2.14 |

## Table 7: Single Axle Load Spectra

| Axle Load (lb) | Vehicle Class | | | | | | | | | |
|---|---|---|---|---|---|---|---|---|---|---|
| | 4 | 5 | 6 | 7 | 8 | 9 | 10 | 11 | 12 | 13 |
| 3,000 | 1.25 | 7.78 | 4.63 | 60.24 | 10.84 | 0.49 | 3.97 | 0.10 | 0.10 | 3.73 |
| 4,000 | 0.75 | 20.95 | 0.38 | 5.98 | 14.59 | 0.78 | 0.80 | 0.29 | 0.22 | 0.84 |
| 5,000 | 1.14 | 30.60 | 2.24 | 1.00 | 25.46 | 1.87 | 0.72 | 1.36 | 1.14 | 2.00 |
| 6,000 | 3.00 | 15.37 | 2.90 | 0.58 | 14.90 | 2.09 | 0.96 | 4.78 | 6.03 | 2.47 |
| 7,000 | 8.21 | 5.68 | 1.97 | 0.56 | 7.45 | 1.48 | 0.99 | 5.82 | 10.20 | 4.92 |
| 8,000 | 11.04 | 4.04 | 4.32 | 0.63 | 6.14 | 2.44 | 2.35 | 6.11 | 10.58 | 6.42 |
| 9,000 | 10.63 | 3.50 | 14.42 | 1.14 | 6.64 | 9.64 | 8.90 | 11.92 | 12.36 | 11.20 |
| 10,000 | 11.93 | 2.94 | 23.48 | 2.59 | 4.91 | 26.73 | 24.41 | 15.40 | 15.91 | 14.99 |
| 11,000 | 13.51 | 2.05 | 21.66 | 3.41 | 2.58 | 30.20 | 27.04 | 11.53 | 12.88 | 12.52 |
| 12,000 | 11.88 | 1.31 | 13.28 | 3.16 | 1.51 | 12.72 | 14.88 | 9.87 | 8.34 | 7.61 |
| 13,000 | 7.66 | 1.07 | 6.32 | 3.12 | 1.19 | 3.19 | 7.05 | 9.27 | 7.58 | 6.67 |
| 14,000 | 5.03 | 0.90 | 2.28 | 2.87 | 0.96 | 1.31 | 3.41 | 7.99 | 6.46 | 5.09 |
| 15,000 | 3.45 | 0.75 | 0.91 | 4.20 | 0.67 | 1.20 | 2.03 | 5.88 | 4.24 | 3.44 |
| 16,000 | 2.58 | 0.60 | 0.47 | 3.60 | 0.50 | 1.35 | 0.96 | 4.08 | 2.01 | 4.46 |
| 17,000 | 2.14 | 0.48 | 0.26 | 1.92 | 0.38 | 1.42 | 0.46 | 2.58 | 1.05 | 3.08 |
| 18,000 | 1.72 | 0.34 | 0.16 | 1.50 | 0.31 | 1.26 | 0.25 | 1.50 | 0.49 | 2.95 |
| 19,000 | 1.23 | 0.29 | 0.12 | 0.97 | 0.21 | 0.83 | 0.21 | 0.81 | 0.20 | 2.21 |
| 20,000 | 0.82 | 0.24 | 0.06 | 0.69 | 0.16 | 0.49 | 0.13 | 0.40 | 0.09 | 1.87 |
| 21,000 | 0.52 | 0.17 | 0.04 | 0.64 | 0.12 | 0.23 | 0.10 | 0.16 | 0.04 | 1.20 |
| 22,000 | 0.31 | 0.13 | 0.03 | 0.39 | 0.08 | 0.11 | 0.09 | 0.07 | 0.01 | 1.23 |
| 23,000 | 0.21 | 0.11 | 0.02 | 0.28 | 0.06 | 0.06 | 0.05 | 0.03 | 0.01 | 0.55 |
| 24,000 | 0.14 | 0.08 | 0.00 | 0.23 | 0.04 | 0.03 | 0.05 | 0.01 | 0.02 | 0.10 |
| 25,000 | 0.12 | 0.08 | 0.01 | 0.25 | 0.04 | 0.02 | 0.05 | 0.01 | 0.01 | 0.10 |
| 26,000 | 0.10 | 0.07 | 0.01 | 0.00 | 0.03 | 0.01 | 0.03 | 0.00 | 0.01 | 0.09 |
| 27,000 | 0.08 | 0.06 | 0.01 | 0.00 | 0.03 | 0.01 | 0.02 | 0.00 | 0.00 | 0.09 |
| 28,000 | 0.07 | 0.06 | 0.00 | 0.04 | 0.03 | 0.01 | 0.00 | 0.00 | 0.00 | 0.00 |
| 29,000 | 0.06 | 0.05 | 0.00 | 0.00 | 0.02 | 0.00 | 0.02 | 0.00 | 0.00 | 0.00 |
| 30,000 | 0.05 | 0.04 | 0.00 | 0.00 | 0.02 | 0.00 | 0.00 | 0.00 | 0.00 | 0.00 |
| 31,000 | 0.05 | 0.04 | 0.00 | 0.00 | 0.02 | 0.00 | 0.02 | 0.00 | 0.01 | 0.00 |
| 32,000 | 0.04 | 0.03 | 0.01 | 0.00 | 0.01 | 0.00 | 0.00 | 0.00 | 0.00 | 0.00 |
| 33,000 | 0.05 | 0.03 | 0.00 | 0.00 | 0.02 | 0.00 | 0.00 | 0.00 | 0.00 | 0.00 |
| 34,000 | 0.04 | 0.03 | 0.00 | 0.00 | 0.01 | 0.00 | 0.02 | 0.00 | 0.00 | 0.00 |
| 35,000 | 0.04 | 0.03 | 0.00 | 0.00 | 0.01 | 0.00 | 0.00 | 0.00 | 0.00 | 0.00 |
| 36,000 | 0.04 | 0.03 | 0.00 | 0.00 | 0.01 | 0.00 | 0.00 | 0.00 | 0.00 | 0.09 |
| 37,000 | 0.03 | 0.02 | 0.00 | 0.00 | 0.01 | 0.00 | 0.00 | 0.00 | 0.00 | 0.00 |
| 38,000 | 0.03 | 0.02 | 0.00 | 0.00 | 0.01 | 0.00 | 0.00 | 0.00 | 0.00 | 0.00 |
| 39,000 | 0.03 | 0.02 | 0.00 | 0.00 | 0.01 | 0.00 | 0.02 | 0.00 | 0.00 | 0.09 |
| 40,000 | 0.03 | 0.01 | 0.00 | 0.00 | 0.01 | 0.00 | 0.02 | 0.00 | 0.00 | 0.00 |
| 41,000 | 0.00 | 0.00 | 0.00 | 0.00 | 0.00 | 0.00 | 0.00 | 0.00 | 0.00 | 0.00 |

## Table 8: Tandem Axle Load Spectra

| Axle Load (lb) | Vehicle Class | | | | | | | | | |
|---|---|---|---|---|---|---|---|---|---|---|
| | 4 | 5 | 6 | 7 | 8 | 9 | 10 | 11 | 12 | 13 |
| 6,000 | 0.76 | 0.00 | 1.61 | 95.47 | 4.18 | 0.75 | 0.49 | 0.00 | 0.09 | 1.04 |
| 8,000 | 1.03 | 0.00 | 5.55 | 0.00 | 8.99 | 1.81 | 0.19 | 0.00 | 0.08 | 1.24 |
| 10,000 | 2.75 | 0.00 | 7.61 | 0.00 | 8.84 | 4.03 | 0.55 | 0.00 | 0.73 | 2.53 |
| 12,000 | 3.07 | 0.00 | 8.75 | 0.00 | 12.56 | 6.97 | 2.93 | 0.00 | 4.44 | 2.95 |
| 14,000 | 4.92 | 0.00 | 16.20 | 0.00 | 17.92 | 9.78 | 4.85 | 0.00 | 10.15 | 4.00 |
| 16,000 | 7.66 | 0.00 | 16.38 | 0.00 | 15.44 | 7.81 | 6.22 | 0.00 | 16.46 | 5.97 |
| 18,000 | 7.18 | 0.00 | 9.27 | 0.00 | 10.97 | 6.04 | 10.70 | 0.00 | 21.34 | 8.47 |
| 20,000 | 6.06 | 0.00 | 4.41 | 0.00 | 7.32 | 5.21 | 11.02 | 0.00 | 21.60 | 11.14 |
| 22,000 | 5.63 | 0.00 | 2.64 | 0.00 | 4.98 | 4.75 | 9.99 | 0.00 | 15.08 | 9.41 |
| 24,000 | 6.08 | 0.00 | 2.25 | 0.00 | 3.41 | 4.54 | 8.19 | 0.00 | 6.71 | 12.12 |
| 26,000 | 7.94 | 0.00 | 2.05 | 0.00 | 2.15 | 4.89 | 8.31 | 0.00 | 2.08 | 11.78 |
| 28,000 | 9.37 | 0.00 | 2.14 | 0.76 | 1.33 | 6.31 | 8.30 | 0.00 | 0.76 | 5.11 |
| 30,000 | 8.93 | 0.00 | 2.62 | 1.19 | 0.72 | 8.85 | 7.70 | 0.00 | 0.25 | 3.85 |
| 32,000 | 6.82 | 0.00 | 3.73 | 0.00 | 0.38 | 10.47 | 6.86 | 0.00 | 0.07 | 4.06 |
| 34,000 | 5.50 | 0.00 | 4.14 | 1.39 | 0.22 | 9.10 | 4.90 | 0.00 | 0.04 | 2.07 |
| 36,000 | 4.79 | 0.00 | 3.91 | 0.00 | 0.17 | 5.34 | 3.07 | 0.00 | 0.04 | 3.33 |
| 38,000 | 3.84 | 0.00 | 2.97 | 0.00 | 0.11 | 2.20 | 2.46 | 0.00 | 0.03 | 4.03 |
| 40,000 | 2.77 | 0.00 | 1.77 | 1.19 | 0.07 | 0.74 | 1.29 | 0.00 | 0.03 | 2.38 |
| 42,000 | 1.99 | 0.00 | 1.01 | 0.00 | 0.03 | 0.23 | 0.55 | 0.00 | 0.00 | 0.70 |
| 44,000 | 1.18 | 0.00 | 0.56 | 0.00 | 0.04 | 0.09 | 0.50 | 0.00 | 0.00 | 0.42 |
| 46,000 | 0.78 | 0.00 | 0.26 | 0.00 | 0.01 | 0.04 | 0.43 | 0.00 | 0.00 | 0.45 |
| 48,000 | 0.39 | 0.00 | 0.10 | 0.00 | 0.03 | 0.02 | 0.22 | 0.00 | 0.01 | 0.39 |
| 50,000 | 0.22 | 0.00 | 0.04 | 0.00 | 0.02 | 0.01 | 0.09 | 0.00 | 0.00 | 0.61 |
| 52,000 | 0.12 | 0.00 | 0.02 | 0.00 | 0.01 | 0.01 | 0.03 | 0.00 | 0.00 | 0.46 |
| 54,000 | 0.11 | 0.00 | 0.02 | 0.00 | 0.01 | 0.01 | 0.10 | 0.00 | 0.00 | 0.00 |
| 56,000 | 0.05 | 0.00 | 0.01 | 0.00 | 0.01 | 0.00 | 0.02 | 0.00 | 0.00 | 0.00 |
| 58,000 | 0.02 | 0.00 | 0.00 | 0.00 | 0.01 | 0.00 | 0.02 | 0.00 | 0.00 | 0.00 |
| 60,000 | 0.01 | 0.00 | 0.00 | 0.00 | 0.01 | 0.00 | 0.00 | 0.00 | 0.00 | 0.69 |
| 62,000 | 0.01 | 0.00 | 0.00 | 0.00 | 0.00 | 0.00 | 0.00 | 0.00 | 0.00 | 0.15 |
| 64,000 | 0.01 | 0.00 | 0.00 | 0.00 | 0.01 | 0.00 | 0.02 | 0.00 | 0.00 | 0.00 |
| 66,000 | 0.00 | 0.00 | 0.00 | 0.00 | 0.00 | 0.00 | 0.00 | 0.00 | 0.00 | 0.00 |
| 68,000 | 0.00 | 0.00 | 0.00 | 0.00 | 0.01 | 0.00 | 0.00 | 0.00 | 0.00 | 0.23 |
| 70,000 | 0.01 | 0.00 | 0.00 | 0.00 | 0.01 | 0.00 | 0.00 | 0.00 | 0.00 | 0.00 |
| 72,000 | 0.00 | 0.00 | 0.00 | 0.00 | 0.01 | 0.00 | 0.00 | 0.00 | 0.00 | 0.00 |
| 74,000 | 0.00 | 0.00 | 0.00 | 0.00 | 0.01 | 0.00 | 0.00 | 0.00 | 0.00 | 0.23 |
| 76,000 | 0.00 | 0.00 | 0.00 | 0.00 | 0.00 | 0.00 | 0.00 | 0.00 | 0.00 | 0.00 |
| 78,000 | 0.00 | 0.00 | 0.00 | 0.00 | 0.00 | 0.00 | 0.00 | 0.00 | 0.00 | 0.00 |
| 80,000 | 0.00 | 0.00 | 0.00 | 0.00 | 0.00 | 0.00 | 0.02 | 0.00 | 0.00 | 0.23 |
| 82,000 | 0.00 | 0.00 | 0.00 | 0.00 | 0.00 | 0.00 | 0.00 | 0.00 | 0.00 | 0.00 |

**Table 9: Dynamic Modulus Data for S3 and S4 Mixes**

| S3 Mix (Dynamic Modulus, psi) | | | | | | |
|---|---|---|---|---|---|---|
| Temp (°F) | 0.1 Hz | 0.5 Hz | 1 Hz | 5 Hz | 10 Hz | 25 Hz |
| 10 | 2,194,482 | 2,395,862 | 2,472,903 | 2,629,875 | 2,688,509 | 2,758,336 |
| 40 | 995,548 | 1,307,273 | 1,464,214 | 1,817,892 | 2,013,348 | 2,025,775 |
| 70 | 306,328 | 494,014 | 571,255 | 822,116 | 901,579 | 948,270 |
| 100 | 86,215 | 126,454 | 156,197 | 255,138 | 301,891 | 361,526 |
| 130 | 40,825 | 51,128 | 60,620 | 86,963 | 121,483 | 153,106 |
| **S4 Mix (Dynamic Modulus, psi)** | | | | | | |
| Temp (°F) | 0.1 Hz | 0.5 Hz | 1 Hz | 5 Hz | 10 Hz | 25 Hz |
| 10 | 1,976,749 | 2,248,836 | 2,361,669 | 2,610,177 | 2,710,590 | 2,836,667 |
| 40 | 761,210 | 1,059,477 | 1,180,146 | 1,404,441 | 1,513,592 | 1,662,424 |
| 70 | 210,084 | 352,080 | 416,131 | 600,179 | 659,885 | 745,122 |
| 100 | 65,742 | 95,197 | 115,086 | 181,825 | 213,554 | 261,165 |
| 130 | 30,947 | 43,577 | 49,294 | 71,907 | 85,008 | 98,958 |

**Table 10: DSR test data on PG 64-22**

| Temperature (°F) | Angular Frequency = 10 rad/sec | |
|---|---|---|
| | G* (Pa) | δ (°) |
| 142 | 6153 | 77 |
| 147 | 3930 | 18 |
| 153 | 2713 | 79 |

**Table 11: SSE and $R^2$ of the Rutting Model for different Calibration Coefficients**

| Trial # | $\beta_{r1}$ | $\beta_{r2}$ | $\beta_{r3}$ | $\beta_{GB}$ | $\beta_{SG}$ | SSE | $R^2$ |
|---|---|---|---|---|---|---|---|
| 1 | 1 | 1 | 1 | 1 | 1 | 0.035 | 0.8941 |
| 2 | 1 | 1 | 0.75 | 1 | 0.5 | 1.015 | -0.0780 |
| 3 | 1 | 1 | 0.9 | 1 | 0.5 | 0.408 | 0.7579 |
| 4 | 1 | 1 | 0.95 | 1 | 0.5 | 0.168 | 0.8661 |
| 5 | 1 | 1 | 1.1 | 1 | 0.5 | 1.087 | 0.9261 |
| 6 | 1 | 1 | 1.2 | 1 | 0.5 | 10.513 | 0.8894 |
| 7 | 2 | 1 | 1 | 1 | 0.5 | 1.218 | 0.9321 |
| 8 | 2 | 1 | 0.75 | 1 | 0.5 | 0.601 | 0.4645 |
| 9 | 2 | 1 | 0.95 | 1 | 0.5 | 0.210 | 0.926 |
| 10 | 2 | 1 | 0.9 | 1 | 0.5 | 0.013 | 0.8941 |

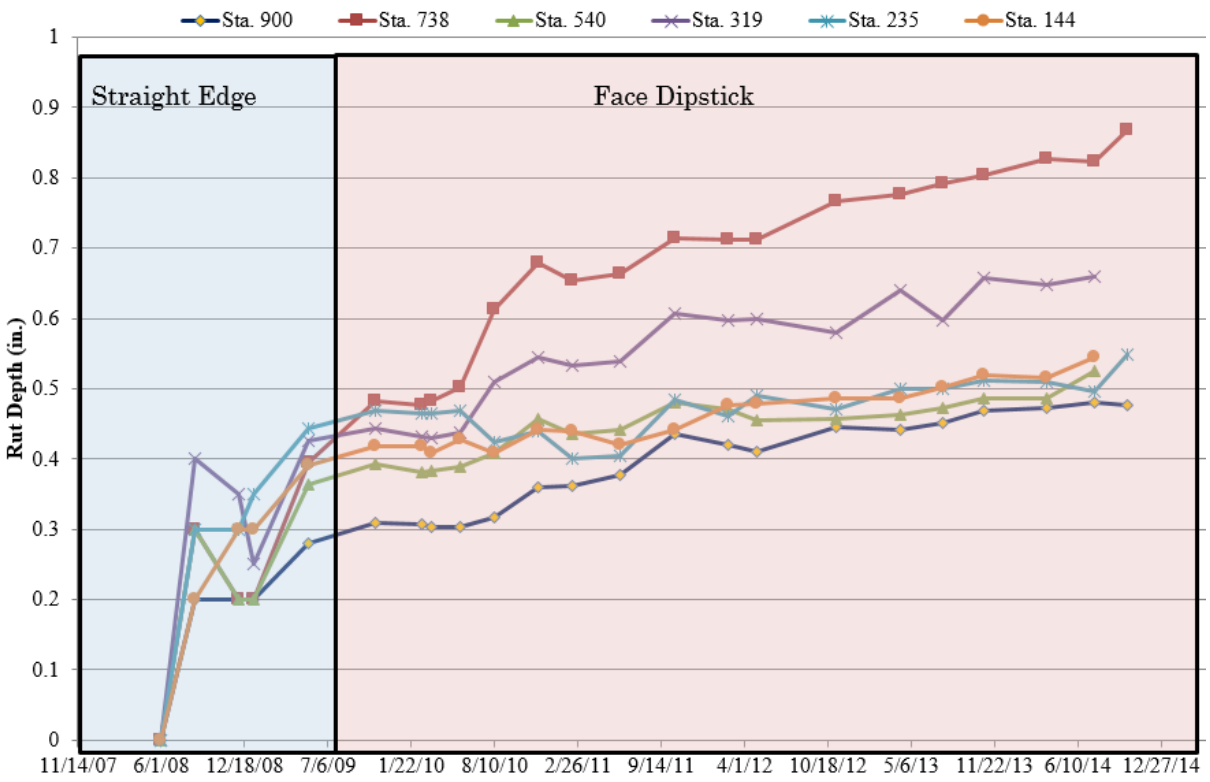


**Figure 1: Rut Progression on the Test Section**

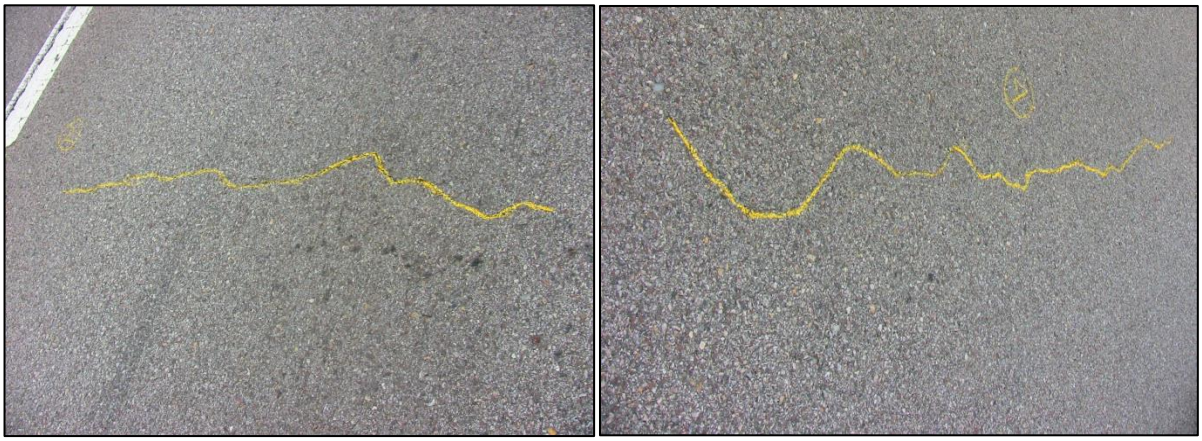

(a) Transverse Crack at 4-ft. from Start (b) Longitudinal cracks from 24-ft to 32-ft.

**Figure 2: Crack Mapping on the Test Section**

(a) (b)

**Figure 3: Marking and Coring to Observe Field Cracking**

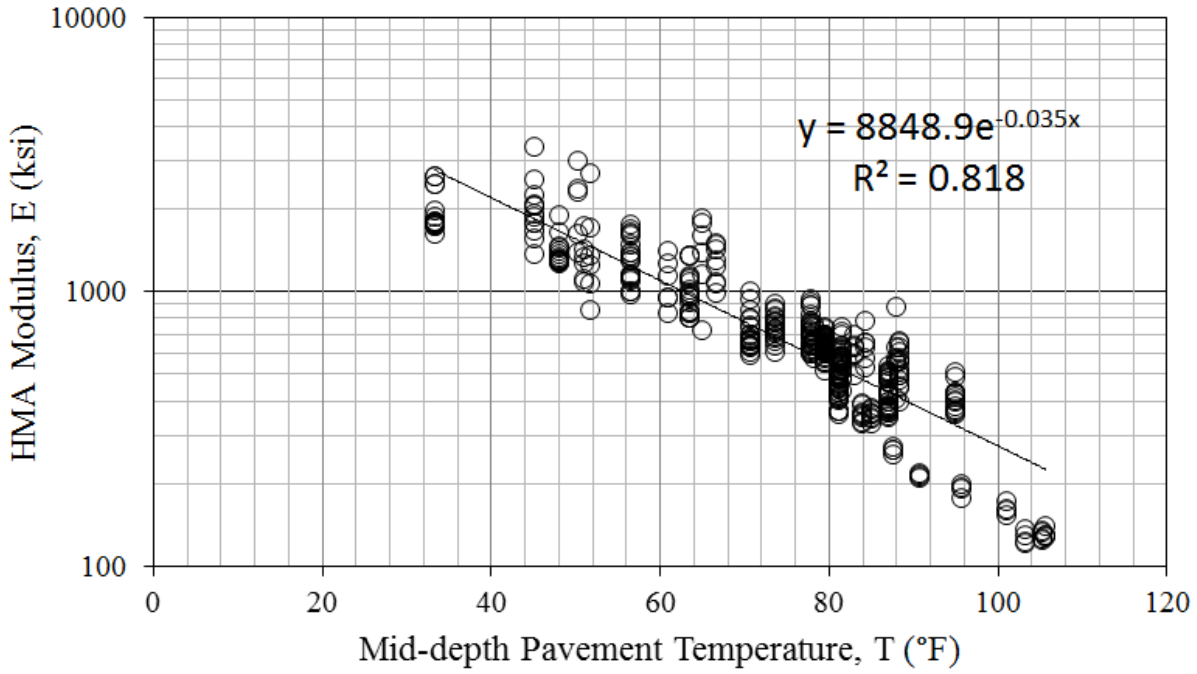


**Figure 4: Asphalt Modulus-Temperature Relationship up to July, 2014**

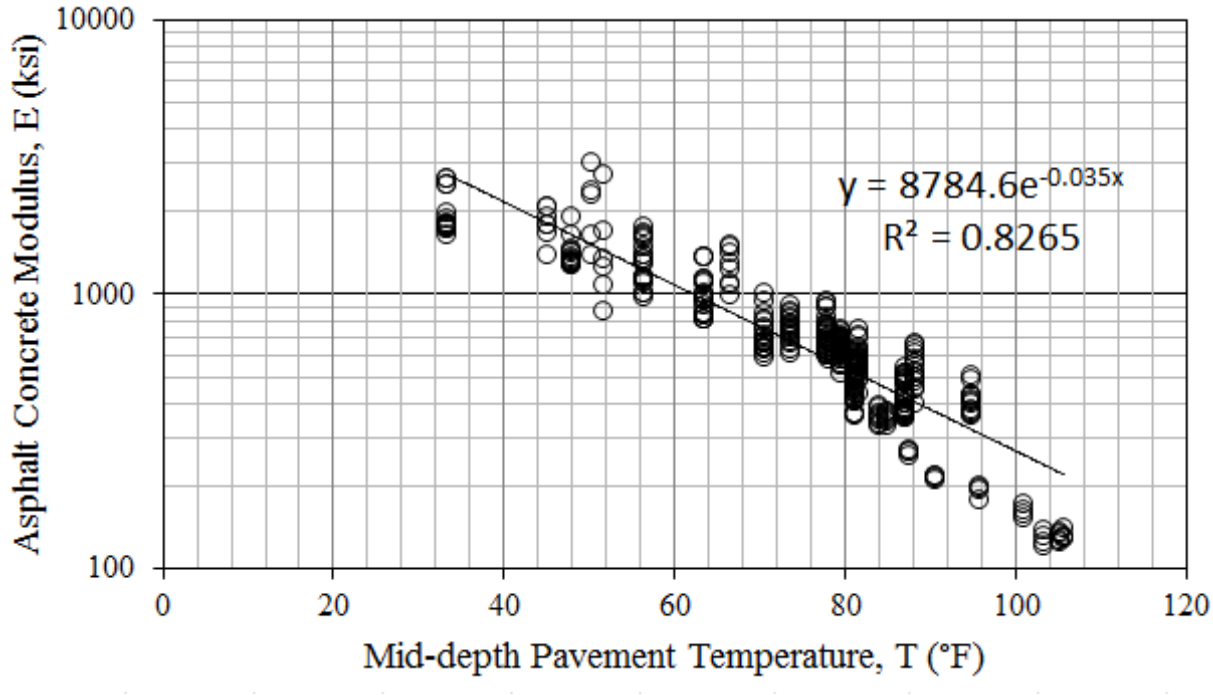


**Figure 5: Asphalt Modulus-Temperature Relationship up to May, 2012**

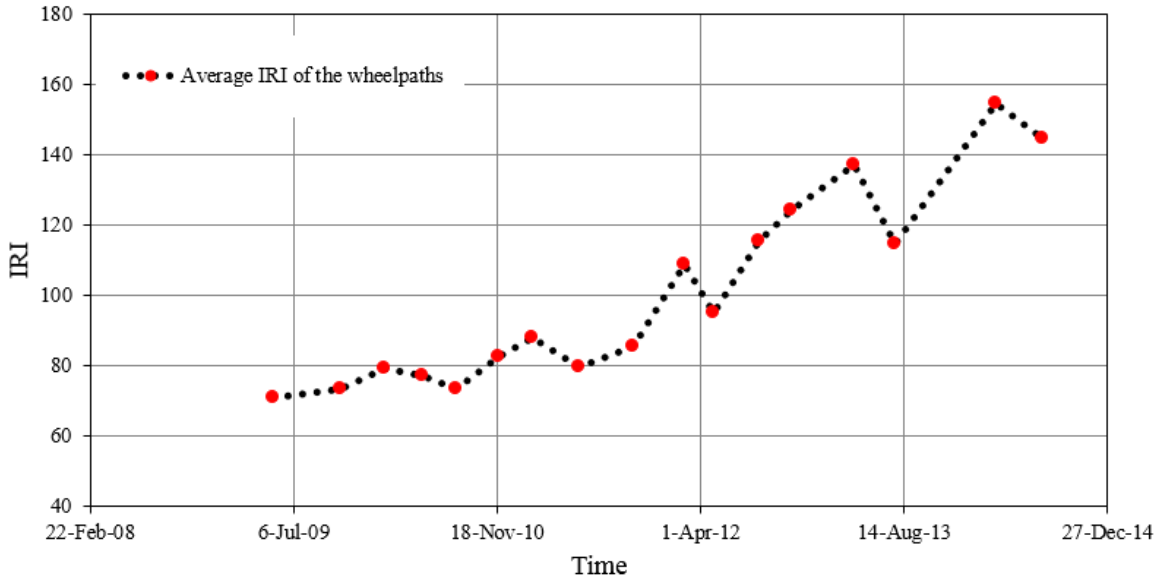


**Figure 6: Average IRI Values for the Test Section**

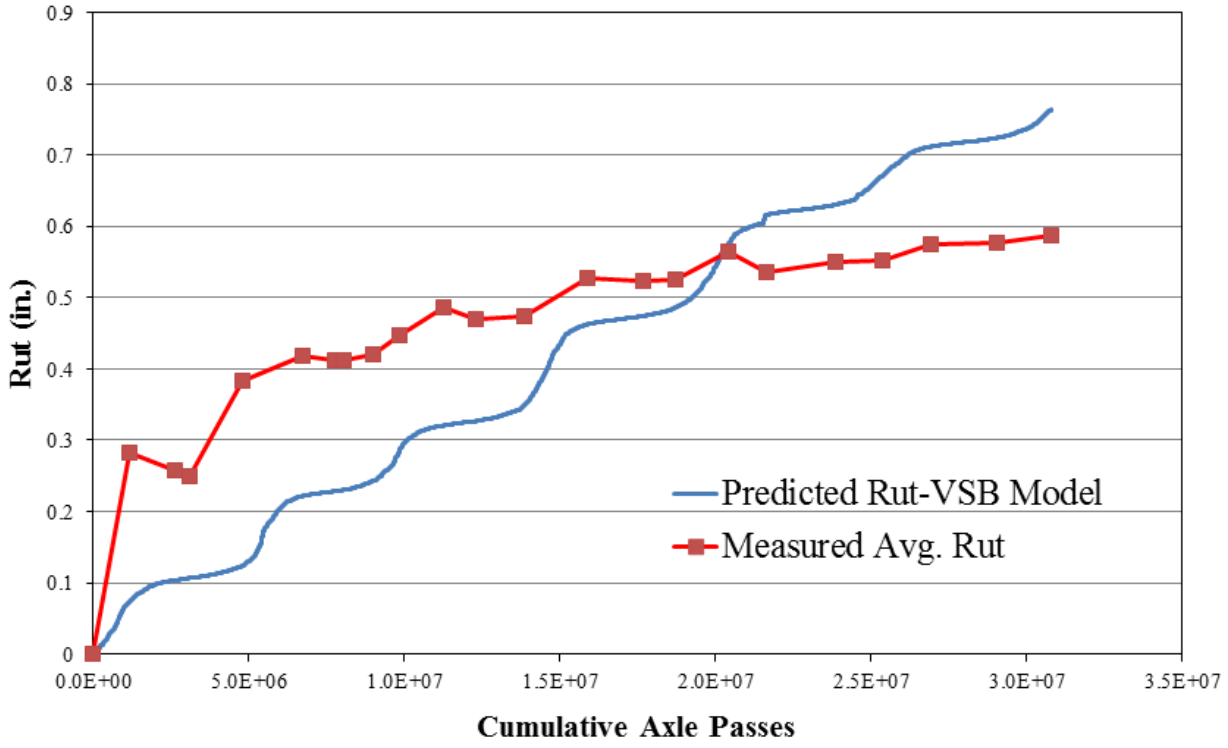


**Figure 7: VSB Rut Prediction Model**

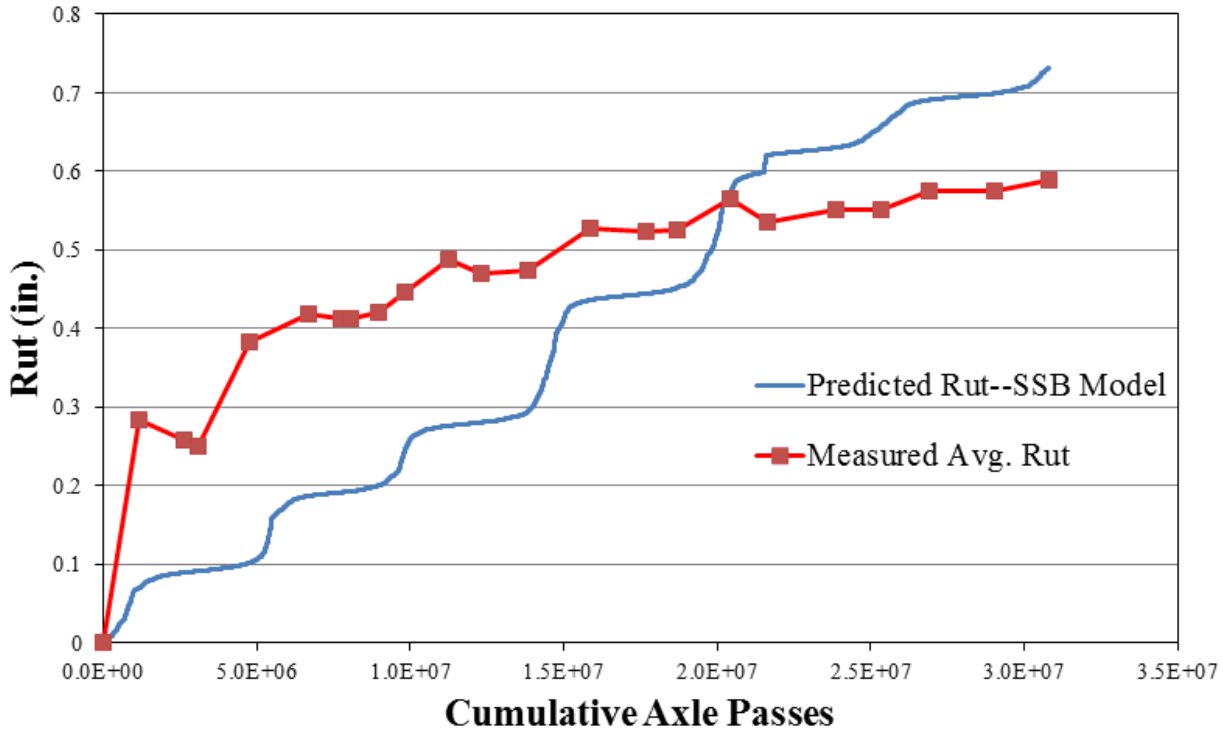


**Figure 8: SSB Rut Prediction Model**

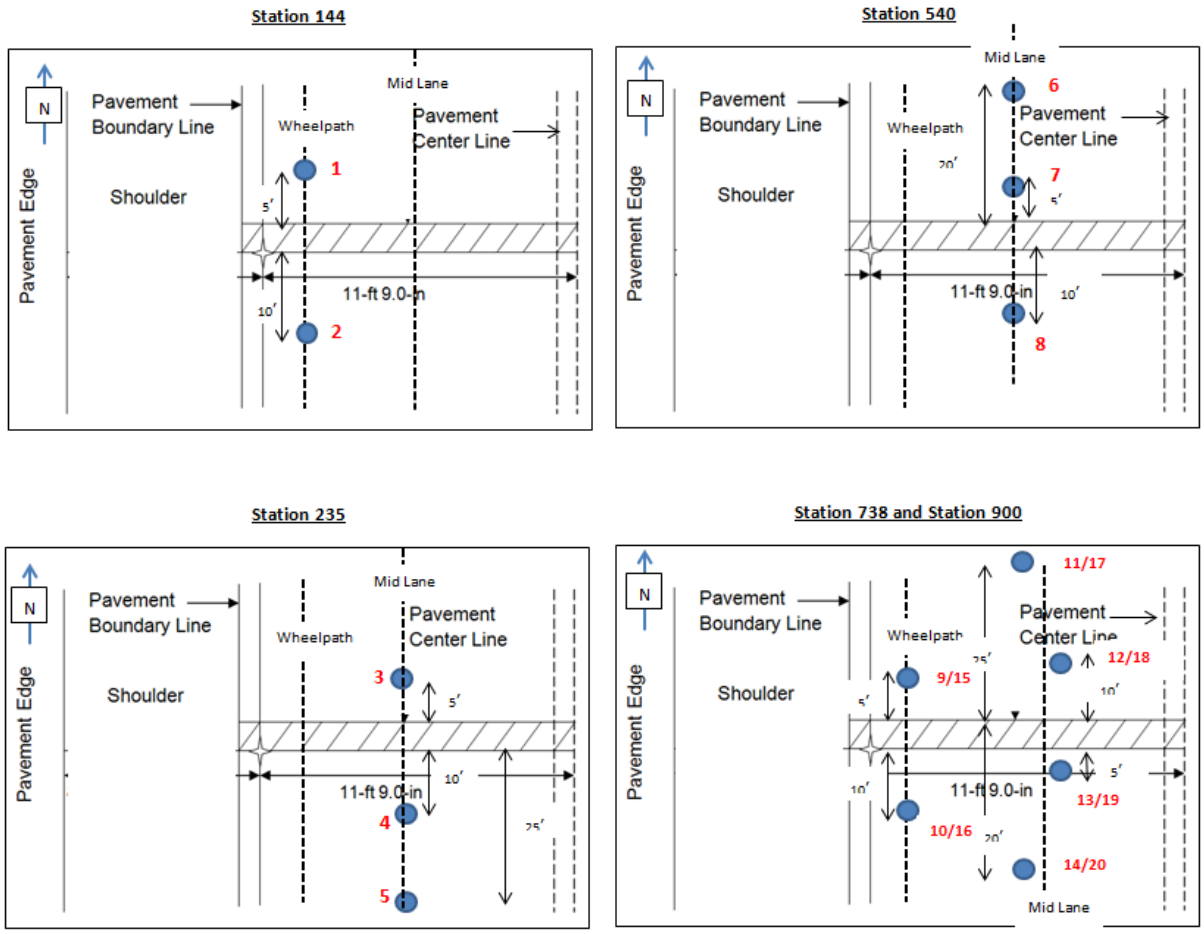


**Figure 9: Core Locations at Different Stations**

**Figure 10: Block Sample Locations at Different Stations**

(a) (b)

**Figure 11: Extraction of Cylindrical Samples from the Test Section**

(a) (b)

**Figure 12: Extraction of Block Samples from the Test Section**


**Figure 13: Hamburg Wheel Tracking (HWT) Testing Device**

**Figure 14: A set of Sample Tested in the HWT**

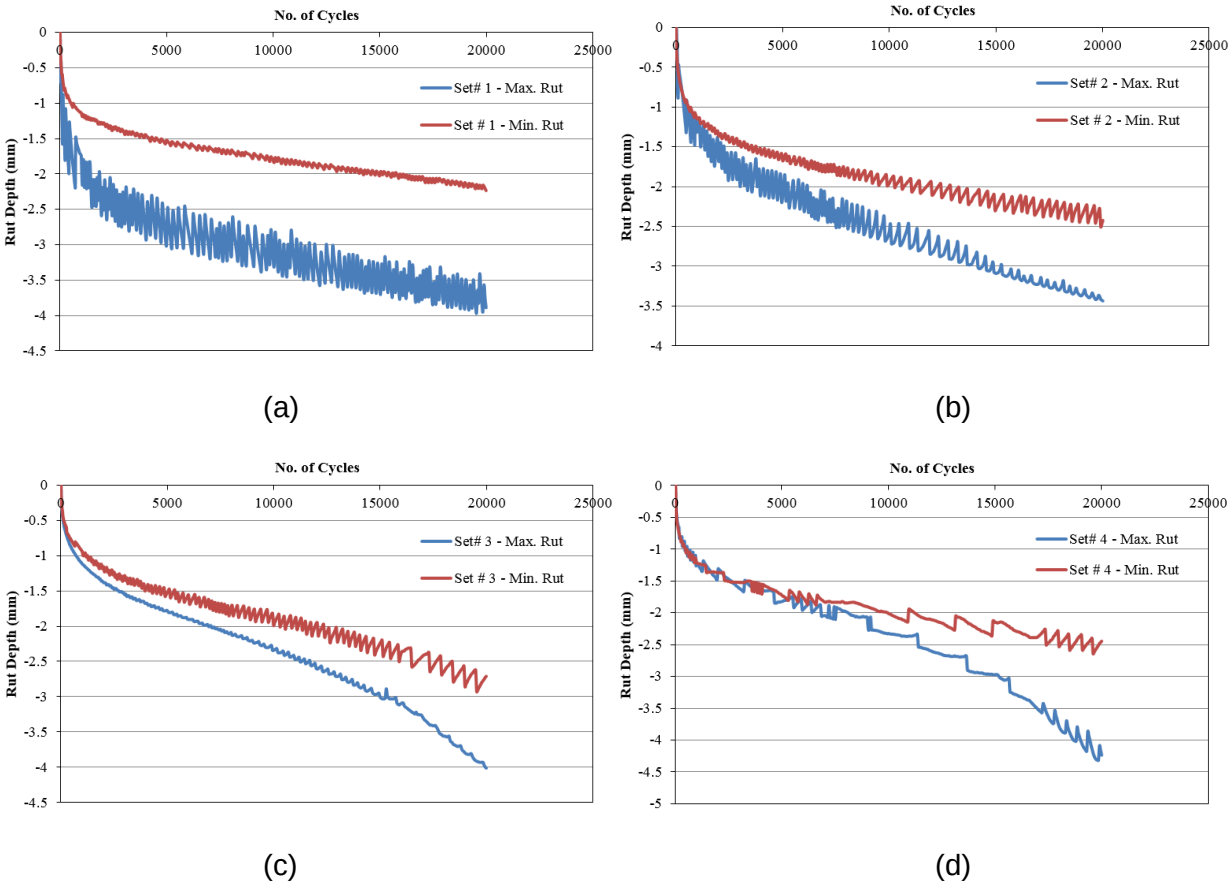


**Figure 15: Rut Tests on Extracted Samples**

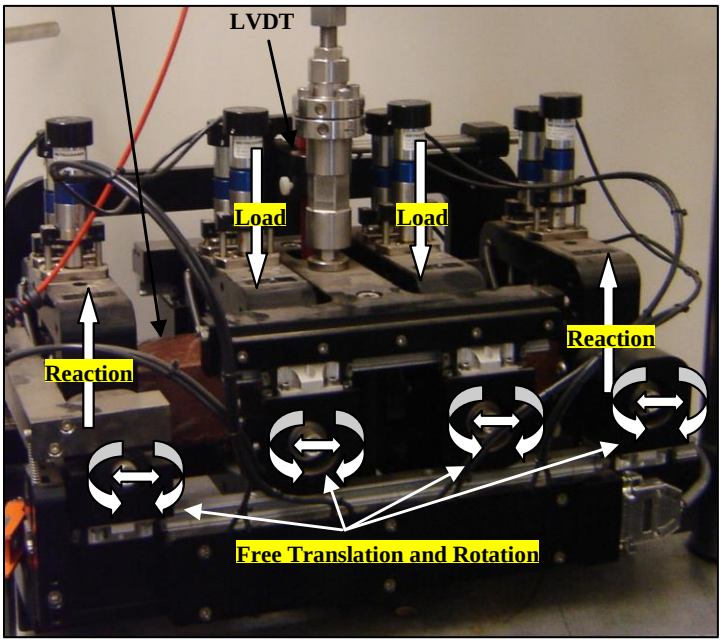


**Figure 16: Setup for Four Point Fatigue Test**

**Figure 17: Fatigue Test Samples**

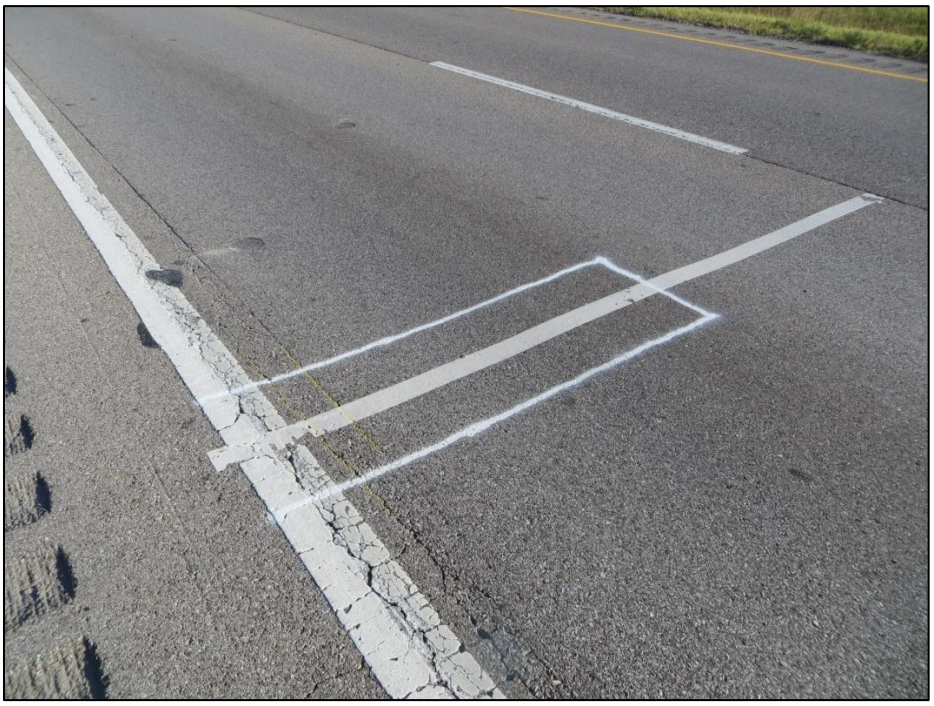

**Figure 18: Marking on the Test Section Before Trenching**

**Figure 19: Cutting of Trench using Saw-cutting Machine**

**Figure 20: Removal of Pavement Materials using Back-hoe**


**Figure 21: Rut Measurements using Face Dipstick®**

**Figure 22: Marking of Different Pavement Layers**

**Figure 23: Depth Measurements of Different Layers**

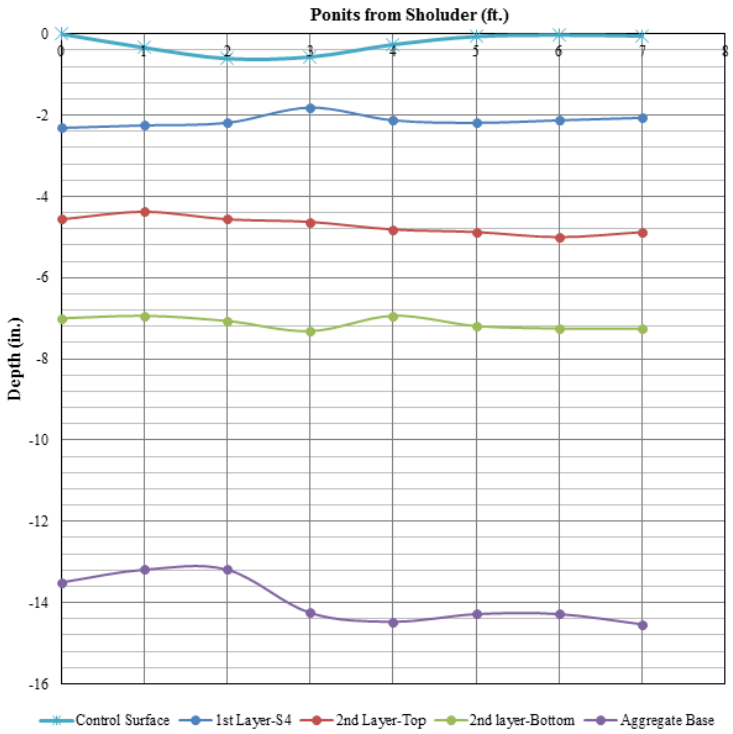


**Figure 24: Average Profile of Pavement layers at Station 235**

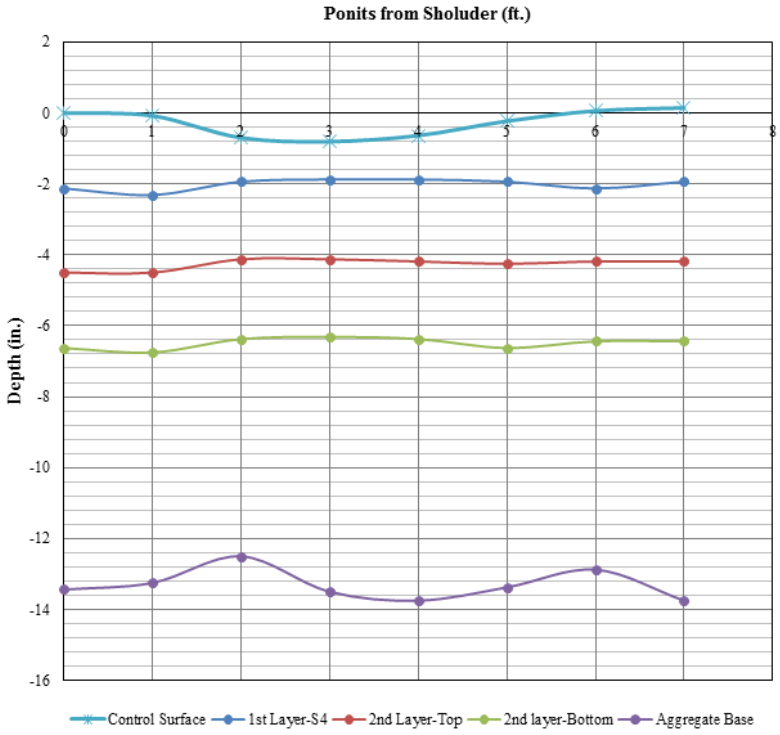


**Figure 25: Average Profile of Pavement layers at Station 738**

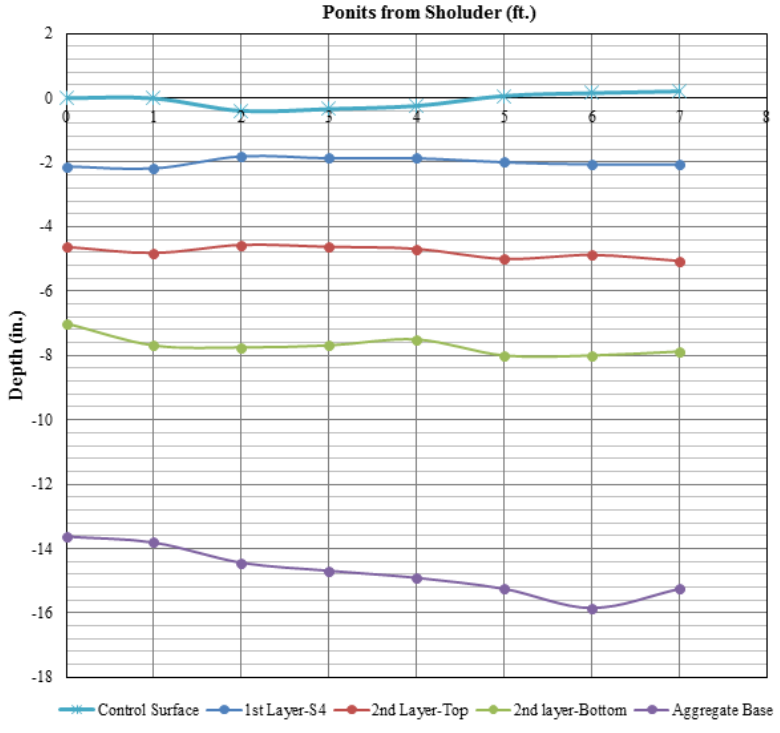


**Figure 26: Average Profile of Pavement layers at Station 900**

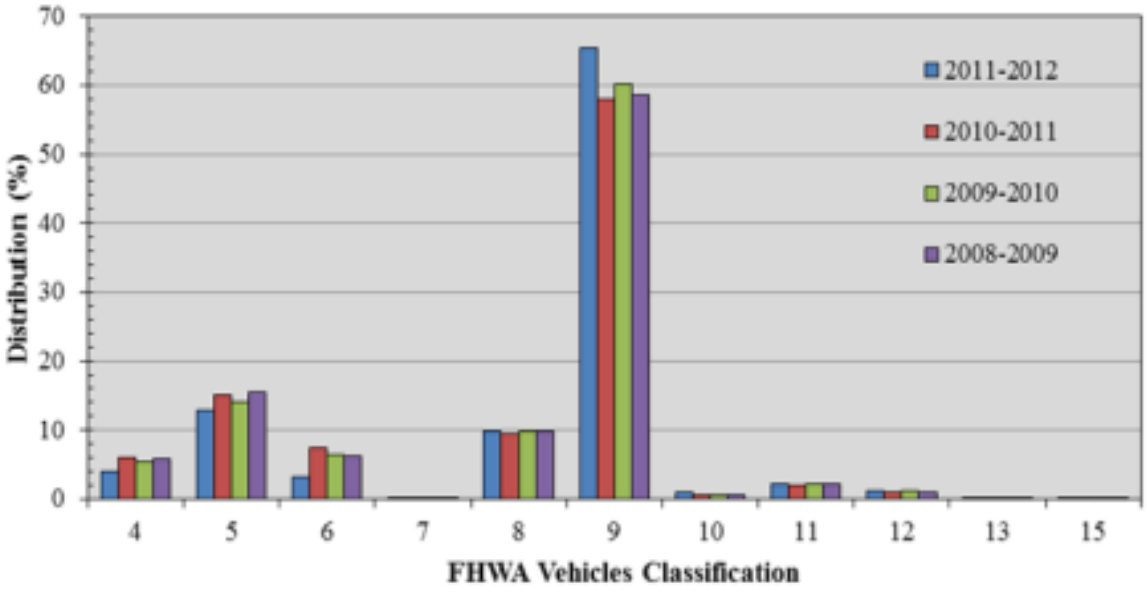


**Figure 27: Vehicle Class Distribution on the Test Section**

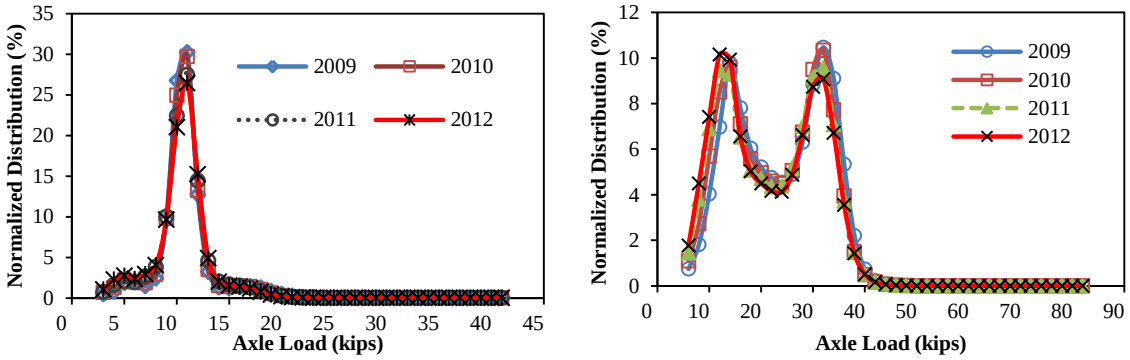


(a) (b)

**Figure 28: Single (a) and tandem (b) ALS for Class 9 vehicles**

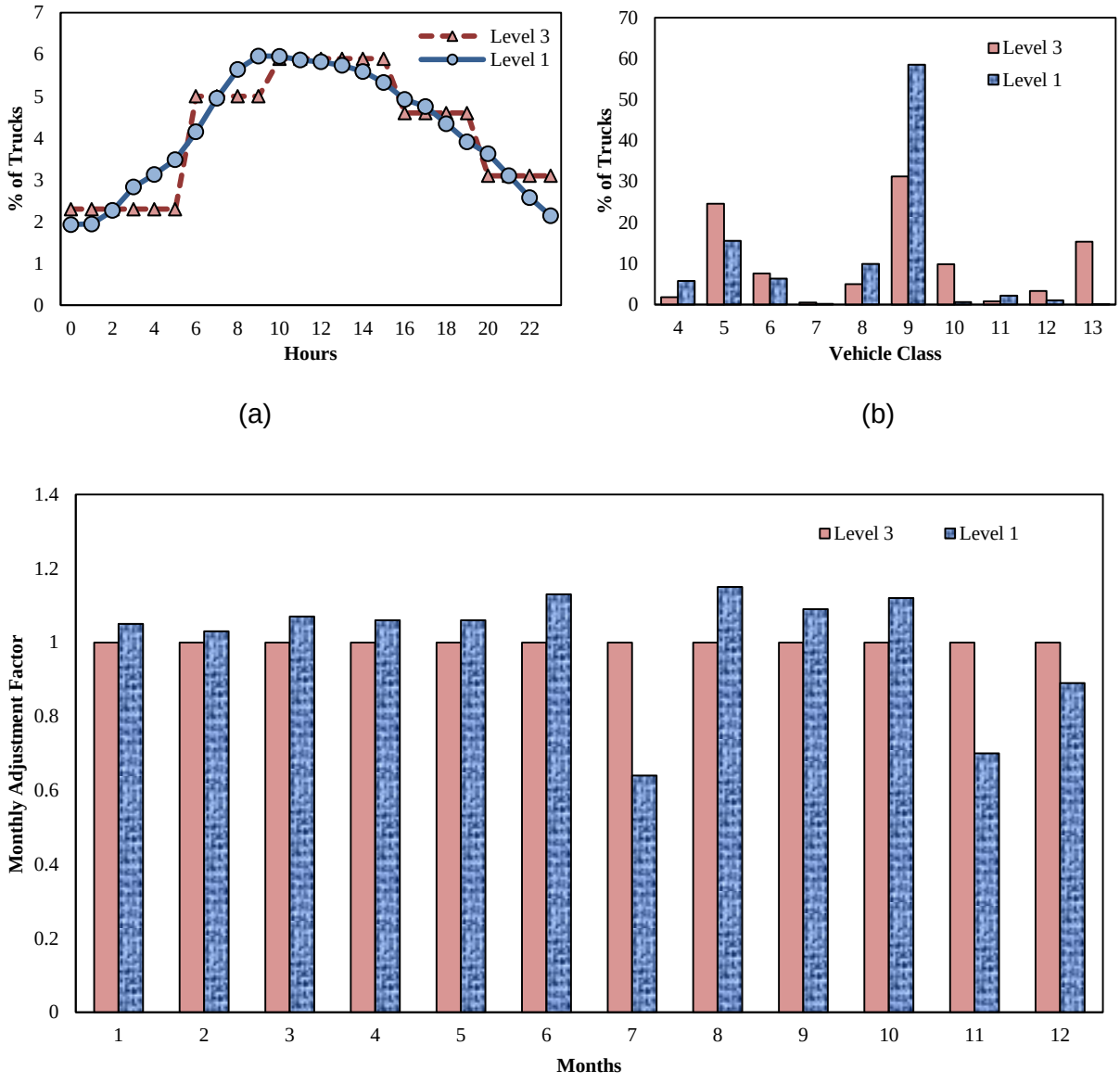


**Figure 29: Comparison of traffic input parameters between Level 3 and Level 1**

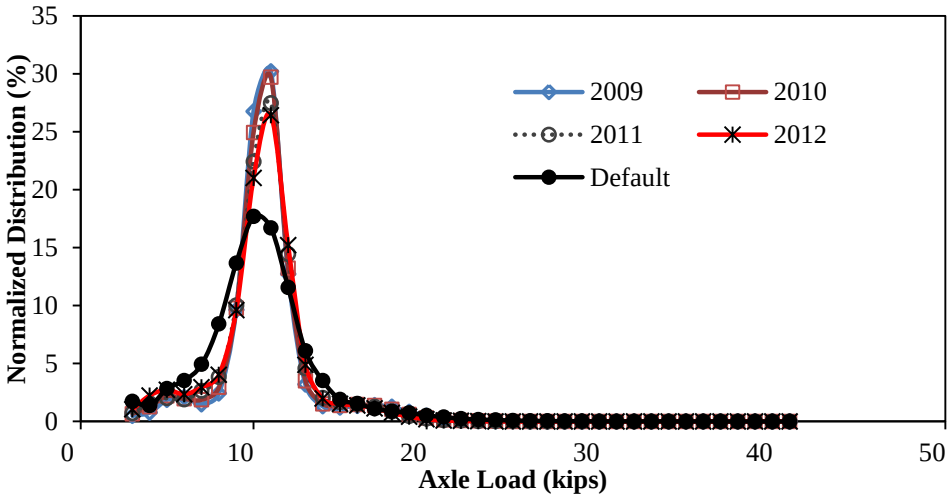


(a)

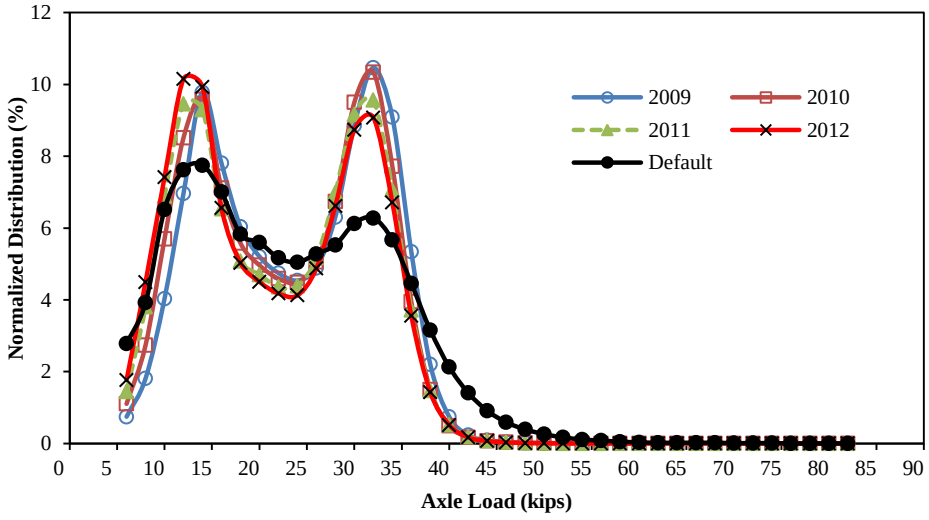


(b)

**Figure 30: Comparison of ALS for Level 3 and Level 1 for (Class 9) (a) single (b) tandem**

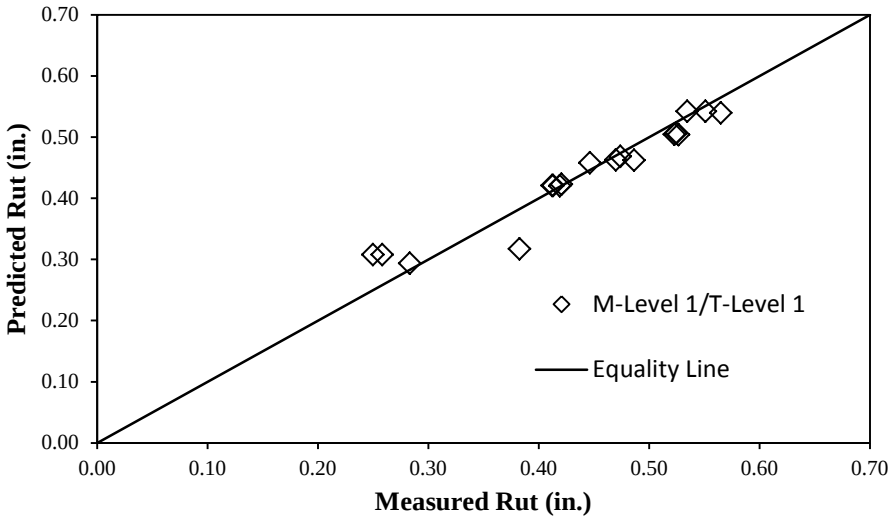


**Figure 31: Measured and Predicted Rut after Calibration**